ANNUAL REVIEWS

Annual Review of Fluid Mechanics

Gas Microfilms in Droplet Dynamics: When Do Drops Bounce?

James E. Sprittles

Mathematics Institute, University of Warwick, Coventry, United Kingdom; email: J.E.Sprittles@Warwick.ac.uk

Annu. Rev. Fluid Mech. 2024. 56:91–118

First published as a Review in Advance on August 22, 2023

The *Annual Review of Fluid Mechanics* is online at fluid.annualreviews.org

https://doi.org/10.1146/annurev-fluid-121021-021121

Keywords

drops, bouncing, wetting, coalescence, air films, impact

Abstract

In the last ten years, advances in experimental techniques have enabled remarkable discoveries of how the dynamics of thin gas films can profoundly influence the behavior of liquid droplets. Drops impacting onto solids can skate on a film of air so that they bounce off solids. For drop–drop collisions, this effect, which prevents coalescence, has been long recognized. Notably, the precise physical mechanisms governing these phenomena have been a topic of intense debate, leading to a synergistic interplay of experimental, theoretical, and computational approaches. This review attempts to synthesize our knowledge of when and how drops bounce, with a focus on (*a*) the unconventional microscale and nanoscale physics required to predict transitions to/from merging and (*b*) the development of computational models. This naturally leads to the exploration of an array of other topics, such as the Leidenfrost effect and dynamic wetting, in which gas films also play a prominent role.

1. INTRODUCTION

The ability of liquid volumes to transition between merging/wetting and bouncing behaviors is common to a myriad of flow configurations. The simple question on which this review is focused is: When do drops bounce? Observations of such phenomena go back at least to the nineteenth century, with Osborne Reynolds noting that water droplets can skate across a liquid surface for a few seconds before merging (Reynolds 1881) and Lord Rayleigh discovering that drops in a jet can bounce off each other (Rayleigh 1899). These historical aspects have been covered in previous reviews (Neitzel & Dell'Aversana 2002, Kavehpour 2015). From a practical viewpoint, understanding when drops bounce is crucial for a range of processes, such as in global climate prediction, where the collision of water droplets governs cloud physics (Grabowski & Wang 2013), or in marine science, where raindrops promote air–sea exchange of minerals and gases (Wanninkhof et al. 2009). Sometimes, one would like to prevent bouncing, such as during a potential nuclear disaster (Hamdan et al. 2015), where drops in a spray need to wet hot rods to cool them, or in multimaterial 3D printing, where drops form the building blocks of complex bespoke objects (Kyobula et al. 2017). However, often, bouncing is to be encouraged, such as in internal combustion engines, where droplets' merging with the wall leads to greater pollutant release (Reitz 2013). These processes, and numerous others, occur across a range of scales, from microdrops in a cloud up to millimetric raindrops, and environments, such as elevated pressures in a combustion chamber (Zhang et al. 2016) down to reduced pressures at altitude, and we would like to understand how these conditions affect the collision outcome.

Whilst Reynolds believed the air to be unimportant, Rayleigh understood that drop merging is related to "whether the air can be anywhere squeezed out during the short time over which the collision extends" (Rayleigh 1899, p. 329), leading him to use different gases to confirm his hypothesis (for further details, see Neitzel & Dell'Aversana 2002). This is by no means obvious, as the relatively low density and viscosity of air, compared to, e.g., water, could, and often has, led one to believe that the air is irrelevant (i.e., dynamically passive). Today, it is widely recognized that the gas has an important role to play. The apparent weakness of air is compensated for by geometrical factors: As a drop approaches another drop or a solid, the air forms a thin layer and it becomes increasingly difficult to squeeze it out; it acts as a lubricant. Ironically, the relevant equations are those of Reynolds (1886). This effect is compounded when droplets become closer and deform, to create flattened surfaces, so that the lubrication force from the air can prevent surfaces from ever contacting and induce bouncing.

In recent times, huge advancements in experimental techniques have enabled collision events to be resolved with unprecedented accuracy, with high-speed cameras capable of temporally resolving millimeter-sized drop-scale dynamics (Thoroddsen et al. 2008). Perhaps most excitingly, an array of new techniques have emerged that resolve the film trapped between impacting surfaces. In many cases, there has been synergistic feedback between experimental and theoretical analyses, with successes in predicting the bubble sizes entrapped under impacting droplets (Josserand & Thoroddsen 2016). Arguably, however, experimental progress is currently ahead of its theoretical counterpart, so that the advantages of the latter, in providing deep understanding of the physical mechanisms at play, resolution of all spatio-temporal scales, and cheap methods for optimizing a process, have not been fully exploited. Recent advances in this direction are the focus of this review.

From a theoretical perspective, the aforementioned phenomena are fascinating and challenging, as the conventional fluid mechanical model (described in undergraduate textbooks) predicts that drops will bounce regardless of the impact speed. The failure to predict merging is because the air/gas film trapped between impacting surfaces reaches the height of micrometers and below, where the conventional model is inaccurate, so that physics usually associated with the microscale

and nanoscale needs to be incorporated to describe a seemingly innocuous macroscopic phenomenon. Without such effects computational observations of merging must be mesh dependent. This review describes how recent advances in modeling and computation have put theory on the cusp of catching up with experimental developments to enable new symbiosis between the two.

In this review it is shown that several drop-related phenomena share the same underlying physics. To isolate the fundamental physics, we focus on head-on collisions of droplets, which for drop–drop cases will be of the same liquid and size, with the resulting dynamics assumed to be axisymmetric. The computation of 3D off-center/oblique impacts requires no additional physics—just a bigger computer! Similarly, an array of interesting topics are sidelined to the Future Issues section, as we focus here on Newtonian fluids with clean interfaces (i.e., no surfactants) and the transition between merging and bouncing, with little interest in postmerging or postbouncing (such as coefficients of restitution for the event) dynamics—again, this is because such aspects can be handled routinely by robust computational frameworks.

ρ_l: liquid density

γ: surface tension coefficient

2. EXPERIMENTAL OBSERVATIONS

Consider a droplet of radius R colliding head on with another droplet of the same radius or impacting a solid (see **Figure 1**) under "isothermal conditions"—a term we use to represent conditions in which evaporation is negligible. Due to the symmetry of the drop–drop problem, we can consider a single droplet impacting a plane of symmetry so that in both cases drops impact a surface (either a plane of symmetry or a solid) at speed U (so that the relative speed in the drop–drop case is $V = 2U$). It is then natural to describe the problem in axisymmetric cylindrical coordinates (r, z, θ). The film thickness, from drop-to-drop or drop-to-solid, is $h(r, t)$ in the lubrication region (so that free surfaces are at $z = \pm h/2$ and $z = h$, respectively). The Weber number in the liquid, $We_l = \rho_l V^2 R/\gamma$, which characterizes how deformed inertial droplets become, is usually considered the primary parameter (in the drop–drop literature this is often based on the diameter $2R$ and so is double the one used here). However, other parameters are important, such as an Ohnesorge number to characterize viscous effects (see **Supplemental Appendix A**: Problem Formulation for details), so that interpreting experiments only in terms of We_l does not give the full picture—even for a given liquid this can be varied using R or V.

Supplemental Material >

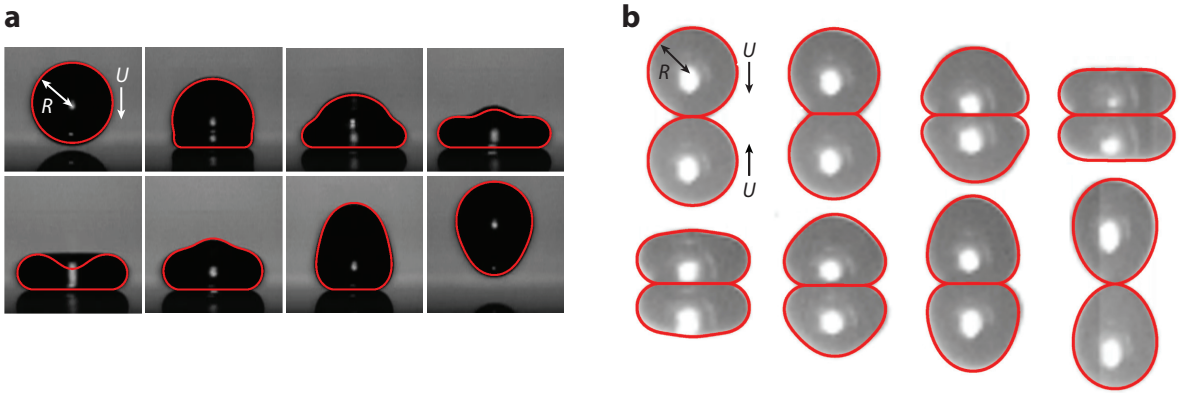

Figure 1

(*a*) Drop–solid bouncing of a silicone oil droplet of radius $R = 0.69$ mm at Weber number $We_l = 2.2$ based on speed U. Panel adapted from de Ruiter et al. (2015b). (*b*) Drop–drop bouncing of a tetradecane droplet with $R = 0.17$ mm at $We_l = 4.7$. Red outlines are our new numerical calculations (see Section 5.5). Panel adapted with permission from Pan et al. (2008).

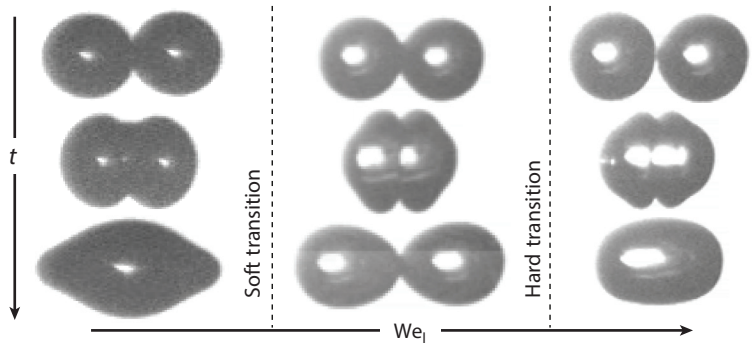

Figure 2

The merge to bounce followed by bounce to merge behavior seen for tetradecane droplets with increasing Weber number We$_l$, leading to two transitions that need to be predicted. At lower We$_l$ the drops remain spherical up to merging, whereas at higher We$_l$ the drops are flattened. Figure adapted with permission from Pan et al. (2008).

2.1. Drop–Drop Bouncing

Let us start with a basic fact: When the gas is removed, colliding drops of the same liquid always merge, as shown by Willis & Orme (2000) with ambient pressure $p_0 \approx 10^{-6}$ atm.

Early experiments considered the collision of water droplets ~100 μm in diameter in air at atmospheric pressure, where coalescence is usually observed for head-on collisions (Qian & Law 1997). However, Jiang et al. (1992) discovered that hydrocarbon droplets display a richer range of outcomes: For low speeds V (or We$_l$) drops merge, at higher V they bounce, and at the highest V they again merge. Hence, there can be two transitions: from merge to bounce (the soft transition) and from bounce to merge (the hard transition) (see **Figure 2**).

2.1.1. Ambient pressure dependence. As seen throughout this review, studying the dynamics of droplets at different ambient gas pressures gives vital clues as to the underlying physics governing the gas film's behavior. Qian & Law (1997) utilized this approach and discovered that by ramping up p_0 water drops could also be made to bounce. For head-on collisions, they found that (*a*) for sufficiently low p_0, the bouncing regime disappears and drops always merge; (*b*) at higher p_0 the bouncing window broadens (i.e., there is a larger range of We$_l$ for which bouncing is observed); and (*c*) gas type is important—for a given p_0 bouncing is more likely in nitrogen than helium.

2.1.2. Recent developments. Experiments have shown that merge–bounce boundaries can also be manipulated by changing the droplet size (Huang & Pan 2021) and viscosity (Al-Dirawi & Bayly 2019). Notably, Huang & Pan (2021) discovered that larger water droplets of $R = 0.5$ mm at atmospheric pressure can also bounce, in the window $1.6 < \text{We}_l < 4.2$.

p_0: ambient pressure in the gas phase

2.2. Drop–Solid Bouncing

Field-wide interest in drop impact was sparked by the surprising discovery of Xu et al. (2005) that lowering p_0, or using a different ambient gas, could suppress drop splashing (see **https://youtu.be/_u-eNgrQOf8**). This led to an explosion of interest in the impact phenomenon and an array of new techniques deployed to understand how the gas influences splashing: Is it caused by the air film prior to contact, after contact, or both, or by some entirely different mechanism?

2.2.1. Discovery of drop bouncing from solids. In 2011–2012 a series of articles used new experimental techniques to reveal the dynamics of the air film, e.g., Driscoll & Nagel (2011), Bouwhuis et al. (2012), and de Ruiter et al. (2012). In particular, Kolinski et al. (2012) described how drops can skate on a film of air before finally contacting the substrate. The discovery of a noncontact drop bouncing came in 2014–2015 from Kolinski et al. (2014) (see **https://youtu.be/Jd54tMI7xFw**) and de Ruiter et al. (2015b) [see supplemental movie 7 from de Ruiter et al. (2015b) for the case from **Figure 1**] and was, arguably, an unexpected outcome of the research into splashing. To be clear, this is a noncontact mode of rebound, in contrast to drop bouncing on superhydrophobic surfaces, where drops spread across hydrophobic pillars. From a side-on view these processes look similar (see **https://youtu.be/XXmOoHEiRCM**) so that imaging from underneath the solid is needed to confirm contact.

2.2.2. Transitions and relations to drop–drop collisions. As in drop–drop collisions, in drop–solid impact the transition between bouncing and merging (i.e., wetting) is often characterized by the Weber number ($We_l = \rho_l U^2 R/\gamma$, as $V = U$). For water drops of radius $R = 1.03$ mm, de Ruiter et al. (2015b) found that bouncing disappears for $U > 0.48$ m/s, corresponding to $We_l \gtrapprox 4$. In Kolinski et al. (2014), a more viscous water–glycerol mixture is used to find $U > 0.75$ m/s, corresponding to $We_l > 7.6$. In the drop–drop terminology, these are the hard (higher in We_l) transitions, and the value for water drops of $We_l \approx 4$ is remarkably close to that seen for drop–drop collisions of $R = 0.5$ mm water drops in Huang & Pan (2021). Interestingly, for $R = 0.35$ mm, no bouncing is seen for drop–drop collisions at any We_l, but drops that are this small are not considered in the drop-on-solid articles.

A soft (lower in We_l) transition is also seen in these experiments—after the drop has performed several bounces it stays near the surface and oscillates gently until eventually wetting it [see supplemental movie 7 from de Ruiter et al. (2015b)]. Replacing impact speed with the vertical speed of the center of mass, de Ruiter et al. (2015b) showed that wetting occurs for $U < 0.02$ m/s, corresponding to $We_l < 0.004$. This is far away from the corresponding soft transition of $We_l \approx 1.6$ seen for drop–drop collisions by Huang & Pan (2021). The reason could be (*a*) that a no-slip solid slows down the gas's drainage (Pan et al. 2009) or (*b*) the different geometries, as in the drop–drop case the gas film is trapped between approaching spheres whereas in the drop–solid case the drop is pressed into the surface by gravity and the film is planar so that the gas is harder to remove.

2.2.3. Phenomenology of the film. In contrast to drop–drop collisions, drop–solid experiments have been able to measure the profile of the gas film trapped between the liquid and solid. This is achieved by observing the process from beneath the substrate, using total internal reflection (TIR) [see **https://youtu.be/Nf810Ompreg** from Kolinski et al. (2014)] or interferometry (de Ruiter et al. 2015b) (see **Figure 3*a***). These experiments show the formation of a dimple in the film at the axis of symmetry whose edge creates a region of relatively high curvature, which we shall refer to as the inner kink—this process, usually followed by touchdown and bubble entrapment, has been discussed in detail by Josserand & Thoroddsen (2016) and often follows the theory presented by Mandre et al. (2009). When this touchdown is prevented, the drop skates over the gas layer, led by an outer kink, creating a relatively flat film between the two kinks (see **Figure 3*a***).

2.2.4. Modes of touchdown. As shown by de Ruiter et al. (2015c) (see **Figure 3*a***), for lower $We_l \lessapprox 1$, the lowest film height is at the outer kink, whereas for $We_l \gtrapprox 1$ it occurs along the film or at the inner kink (where touchdown is usually seen for higher-speed impacts, such as those associated with splashing). The result is two modes of contact, the outer kink mode, associated with prolonged skating, and the film mode, associated with more rapid touchdown.

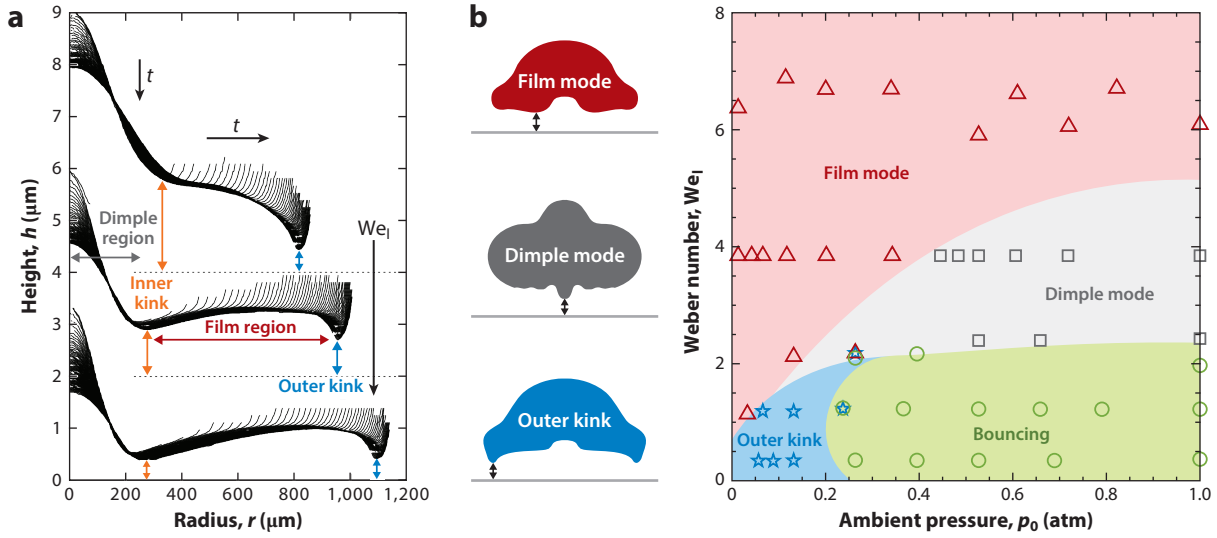

Figure 3

(*a*) Film phenomenology of millimeter-sized water drops as the Weber number We_l is increased, with two sets of curves shifted vertically to allow for easy comparison, and (*b*) different regimes (*colored regions*) of contact observed as the ambient pressure p_0 is lowered for water drops of radius $R = 0.93$ mm. Panels adapted with permission from (*a*) de Ruiter et al. (2015c) and (*b*) Zhang et al. (2021a).

A notable difference between the findings of Kolinski et al. (2014) and de Ruiter et al. (2015b,c) is, for impacts above the hard transition, the characteristic film height observed just before contact. Kolinski et al. (2014) showed heights of ≈2 nm before contact and commented that these values "are far less than those predicted for the onset of instability in thin viscous films" (p. 5), whereas de Ruiter et al. (2015c) noted "sudden collapse of the air layer" when the "film thickness decreases below ∼200 nm" (p. 11)—two orders of magnitude larger!

One way to ensure the smoothness of the underlying substrate is to coat it with a layer of liquid, which is sufficiently thin or viscous that it mimics impact on a smooth solid (Lo et al. 2017; Pack et al. 2017; Zhang et al. 2021a,b). This is known to improve the repeatability of experiments and the stability of air films to encourage skating (Li et al. 2015, Langley & Thoroddsen 2019) by masking the solid's roughness. Notably, this allowed Pack et al. (2017), and later Zhang et al. (2021a,b), to discover a new dimple mode where surface waves focus under the center of the drop to produce touchdown, often in a complex interplay with air bubble entrapment and jetting. This mode only existed for low viscosity liquids, as the waves are damped for more viscous ones [see video in supplemental material of Zhang et al. (2021b)].

2.2.5. Ambient pressure dependencies. Zhang et al. (2021a) performed the equivalent experiment to that of Qian & Law (1997) for drops impacting film-coated solids and explored the influence of ambient pressure p_0 on transitions. As the film's dynamics can be captured, the regime diagram, shown in **Figure 3*b***, is also able to identify the modes of contact. To summarize, these authors found, very similar to the drop–drop case, that (*a*) for sufficiently low p_0, the bouncing regime disappears and drops always merge; (*b*) at higher p_0 the bouncing window initially broadens (i.e., there is a larger range of We_l for which bouncing is observed); and (*c*) the outer kink mode seen for drop-on-solid impact is now only recovered at reduced p_0.

2.3. Drop Impact on a Film/Bath/Sessile Drop

It is relevant to make some comments on other drop–surface collisions. Since the work on hydrodynamic quantum analogs (see **https://youtu.be/sGCtMKthRh4** and Bush 2015), the community has become acutely aware that air films can prevent droplets from contacting liquid baths in special circumstances (e.g., a vibrated surface). Notably, even in the absence of oscillations, drops can sometimes float on a surface for ∼30 min (Couder et al. 2005). Physically, there is little to add to what has already been said, although typically we now have more parameters. As one may expect, a gas cushion between the impacting droplet and the surface beneath causes interfaces to deform and the coalescence to be delayed (i.e., drops can appear to temporarily float or rebound). Subsequent coalescence has been covered by Kavehpour (2015).

2.3.1. Impact on an initially planar surface. The limiting cases correspond to a very thin, undeformable liquid film, which has more in common with drop impact on a solid, and a deep bath, where the presence of the lower solid is irrelevant and the deformation of the bath is often more extreme than the drop's. Varying the film thickness between these limits leads to a rich variety of behaviors. With regards to transitions, which are our focus, Pan & Law (2007) and Tang et al. (2016) showed that for some fixed Weber numbers, increasing the film height can lead to fascinating transitions from merging to bouncing to merging, and to bouncing again. Furthermore, Pan & Law (2007) discussed how the contact position varies with parameters, and Duchemin & Josserand (2020) considered gravity-driven drainage. Later work characterized the gas film's behavior using interferometry (Tang et al. 2019) and considered a detailed parametric study of the system (Sanjay et al. 2022). Recent articles have extended the basic cases to consider the case where the film/bath and the drop are different liquids (Cuttle et al. 2021, Wu & Saha 2022).

2.3.2. Impact on a curved surface. A drop impacting a sessile drop on a solid has also been considered (e.g., Abouelsoud & Bai 2021), where solid wettability (i.e., sessile drop shape) becomes important. A map of bounce–merge transitions is given by Moon et al. (2018).

2.3.3. Ambient pressure dependence. It has long been known that the ambient gas conditions alter the merging behavior (Schotland 1960). For example, Bach et al. (2004) considered the impact of microdrops with a bath and demonstrated changes in the bounce–merge transition when varying p_0 or the ambient gas used.

3. CONVENTIONAL FLUID MECHANICAL DESCRIPTION

There are several modeling frameworks that could be considered, such as molecular dynamics or kinetic theory for the gas, but these microscopic/mesoscopic approaches are, at present, computationally intractable for the phenomena we are interested in. They can, however, provide vital information that can be fed into a macroscopic model based on the Navier–Stokes–Fourier (NSF) paradigm (Shikhmurzaev 2007) to extend the conventional accuracy of this model; this is the approach we take. The main ideas are described here, focusing on the equations for a gas lubrication model, while in **Supplemental Appendix A**: Problem Formulation, we provide full mathematical descriptions for the models introduced and identify dimensionless parameter groups. Initially, we consider the isothermal case.

Supplemental Material >

3.1. Full Navier–Stokes Model

Conceptually, the simplest approach is to solve the incompressible Navier–Stokes equations (NS equations) in the liquid and gas. Then, the full problem formulation requires boundary conditions: conventionally, at liquid–gas interfaces, that the velocity is continuous, viscous stress from the

fluids balances with capillary stress, and there is a kinematic equation, and at liquid–solid interfaces, that we have no slip. The initial condition requires the shape (which is usually assumed to be a sphere) and velocity profile (which is typically uniform with speed U in the liquid) of the drop.

μ_g: gas dynamic viscosity

3.2. Navier–Stokes-in-Liquid with Lubrication-in-Gas Model

Due to the relatively low gas-to-liquid viscosity ratio, the gas only deforms the drop when thin films are formed and lubrication forces are generated (see Section 3.3 for estimates). Therefore, a popular approach is to solve the NS equations in the liquid (or some variant thereof) coupled to a lubrication model for the gas—outside the lubrication region the gas is assumed to be dynamically passive. Considering simultaneously drop–drop and drop–solid cases, so that their similarities become clear, if $U_r(r, t)$ is the radial speed of the liquid at the gas–liquid interface, then the usual lubrication approach, based on the incompressible NS equations, assuming inertia is negligible in the film, gives

$$\frac{\partial h}{\partial t} + \frac{1}{r}\frac{\partial (rQ_r)}{\partial r} = 0, \tag{1a.}$$

$$Q_r = \underbrace{\frac{-h^3}{12\mu_g}\frac{\partial p_g}{\partial r}}_{\text{Poiseuille}} + \underbrace{fhU_r/2}_{\text{Plug/Couette}}, \tag{1b.}$$

where $f = 2$ for the drop–drop case (with plug flow) and $f = 1$ for the drop–solid case (Couette flow) (see **Figure 4*a***). Alongside the normal stress, which is dominated in the gas film by p_g, the drop's boundary conditions require knowledge of the shear stress:

$$\tau_g = \frac{h}{2}\frac{\partial p_g}{\partial r} + (2 - f)\frac{\mu_g U_r}{h}. \tag{2.}$$

This model operates as a surface differential equation for the liquid drop's dynamics that calculates the stress the drop feels from the gas in the lubrication region. Notably, the parameterization of the free surface as $h = h(r, t)$ will fail to describe the whole drop, but it will capture the lubrication region, and as we shall discover, we are usually in a fortuitous case where gas pressures are only significant in thin regions, where our model is most accurate.

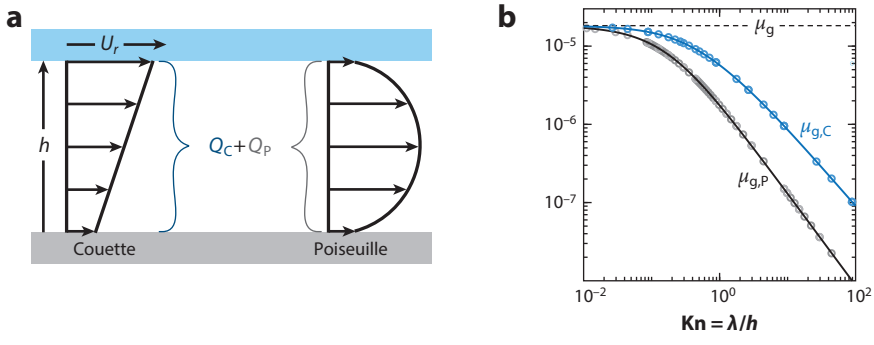

Figure 4

(*a*) Decomposition of the gas layer's dynamics into a mass flow rate from Couette Q_C and Poiseuille Q_P components. (*b*) Fits for the effective viscosities $\mu_{g,P}$ and $\mu_{g,C}$ (see Equations SB1a and SB1b), as a function of Knudsen number $\mathrm{Kn} = \lambda/h$, that capture calculations from the Boltzmann equation (*symbols*) (for details, see Chubynsky et al. 2020). Panel *b* adapted from Chubynsky et al. (2020) (CC BY 4.0).

3.3. Paradoxes: Insight from Rigid-Sphere Models

A key focus in the early literature of drop–drop collisions was on meteorological applications where droplets are typically ∼10–100 μm and the assumption that they remain approximately spherical during impact is more reasonable, as surface forces dominate volumetric ones (of viscosity or inertia). In particular, the Stokes and inertial drag on the spheres (creating pressure $\sim\mu_g V/R$ and $\sim\rho_g V^2$) is weak during approach compared to the capillary pressure $\sim\gamma/R$, so that $\mathrm{Ca}_g = \mu_g V/\gamma \ll 1$ and $\mathrm{We}_g = \rho_g V^2 R/\gamma \ll 1$. For example, for a drop of water of $R \sim 10$ μm at standard ambient conditions, the terminal velocity for falling under gravity is $V_{\text{terminal}} \sim 10^{-2}$ m/s so that $\mathrm{Ca}_g \sim 10^{-6}$ and deformation only kicks in at $h \sim R\sqrt{\mathrm{Ca}_g} \sim 10$ nm. Furthermore, in this initial stage, before deformation, given the small gas-to-liquid viscosity ratio ($\mu_g/\mu_l \ll 1$), one can think of rigid spheres (i.e., no slip abiding, for the gas; see Davis et al. 1989) and expect the lubrication model to be valid. This simplified arena is interesting for us, as it has led to several breakthroughs in understanding and the development of models incorporating unconventional physics.

ρ_g: gas density

μ_l: liquid dynamic viscosity

These considerations demarcate drop collisions in gas from those in liquid, where μ_g typically takes larger values, so that the drops feel each other hydrodynamically, so to speak, well before reaching a lubrication regime. Mathematically, this makes the drop-in-liquid case more complex. Computationally, however, drop-in-gas is potentially worse due to the multiscale nature of the phenomenon.

3.3.1. Analytical results for rigid spheres. Early works focused on the atmospheric (cloud physics) problem of knowing when colliding droplets will merge and when they will bounce, giving the so-called collision efficiency. This work commenced with Hocking (1959), who considered spheres sedimenting and assumed Stokes flow; this work was refined by Davis & Sartor (1967), based on expressions from Stimson et al. (1926), and then by Hocking & Jonas (1970). In these articles, the conventional model was used and shown to prevent contact of rigid spheres, with $U_r = 0$. In particular, local to $r = 0$, the height is approximately parabolic, $h(r, t) = h_0(t) + r^2/R$ [so $h_0(t) = h(0, t)$], and $\partial h/\partial t = -v$, so that with $U_r = 0$, using Equation 1a,b, with $\partial p_g/\partial r|_{r=0} = 0$ and $p_g(r \to \infty) \to p_0$, we find

$$p_g - p_0 = \frac{3\mu_g v R}{2(h_0 + r^2/R)^2}.$$

Integrating the pressure over the surface gives a singular repulsive force proportional to h_0^{-1}. Consequently, an artificial merging height was introduced, and Hocking & Jonas (1970) commented, "the collision efficiencies of droplets of radius less than 20 μm is shown to vary considerably with the critical minimum gap between the droplets below which collision is assumed always to occur" (p. 722).

3.3.2. Analytical results for flat interfaces. Deformation makes matters worse, as the film flattens and it becomes even harder for the gas to escape and initiate merging. Here, one can imagine two no-slip planar [$h = h_0(t)$] discs of radius R with $\partial h/\partial t = -v$, $\partial p_g/\partial r|_{r=0} = 0$, and $p_g(r = R) = p_0$ to find

$$p_g - p_0 = \frac{3\mu_g v}{h_0^3}(R^2 - r^2)$$

and, hence, a more singular force, which is proportional to h_0^{-3}.

4. BEYOND CONVENTIONAL LUBRICATION: EXTRA PHYSICS

The conventional framework fails. Not only is contact prevented, as confirmed by simulations with deformable interfaces (see Section 4.1), but variations in ambient gas pressure cannot

influence droplet dynamics, most notably moving merging–bouncing transitions. This is because the pressure can be considered with respect to p_0, meaning that this parameter drops out of the model entirely, so that the gas is characterized only by its viscosity, which does not depend on p_0 and, furthermore, varies little for the different gases used in experiments.

This section considers various candidates for the missing physics, which we see fits best into a lubrication framework for the gas.

4.1. Intermolecular van der Waals Forces

Films on solids or free liquid films are destabilized at sufficiently small scales by van der Waals (vdW) forces, which can drive interfaces into contact. For the collision of liquid drops in a liquid medium, the incorporation of this physics is commonplace (see Chan et al. 2011). Within a lubrication framework, vdW forces can appear as a disjoining pressure,

$$p_{\mathrm{d}} = -\frac{A}{6\pi h^3}, \qquad 3.$$

that acts on each interface. Here A is the Hamaker constant for the particular liquid–gas–liquid or solid–gas–liquid system considered, typically of the order of 10^{-21}–10^{-18} J.

The importance of this force has also been discussed for collisions in a gas, including for drop-on-drop (Pan et al. 2008, Li 2016) and drop-on-solid (Kolinski et al. 2014) cases. Notably, simulations of drop–drop collisions by Pan et al. (2008) and drop–solid ones by Chubynsky et al. (2020) demonstrate that vdW forces are required for contact, but that the values of $\mathrm{We_l}$ obtained for the transitions are wildly different from those observed in experiments (see Section 5.4.1 for details). Both articles consider gas kinetic effects (GKE) as crucial to predicting transitions by reducing the film height to scales at which vdW forces are relevant (typically ∼10 nm; see Chubynsky et al. 2020) and merge the interfaces.

4.2. Gas Kinetic Effects

The conventional formulation loses accuracy when the mean free path in the gas λ becomes comparable to relevant length scales in the problem—for us, the characteristic film height—after which the Boltzmann equation is required for accurate solutions. For air at atmospheric pressure ($p_{\mathrm{atm}} \approx 10^5$ Pa) we have $\lambda \approx 70$ nm, so that once film heights reach ∼100 nm, which is routinely achieved, we expect GKE to become important.

The introduction of GKE was first considered to overcome the paradox in the collision of rigid spheres. Specifically, Davis (1972) and Hocking (1973) incorporated a Maxwell slip condition, valid for small Knudsen numbers $\mathrm{Kn} = \lambda/h$, at the gas–sphere boundary that permitted contact in finite time, thus removing the need for an artificial cutoff with a physical parameter. Sundararajakumar & Koch (1996) went beyond the small Kn assumption using the linearized Boltzmann equation in a lubrication framework. Extensions of rigid sphere work to nonaxisymmetric collisions have recently been provided by How et al. (2021), as have considerations of the effect of internal flow by Ababaei & Rosa (2023).

As shown in the sidebar titled Modeling Gas Kinetic Effects: Flow in a Channel, for a lubrication problem GKE can be neatly wrapped up in effective viscosities, which are functions of the local Knudsen number, $\mathrm{Kn}(r, t) = \lambda/h(r, t)$. Two effective viscosities have to be introduced, one associated with Poiseuille flow, $\mu_{\mathrm{g,P}}(\mathrm{Kn})$, and the other for Couette flow, $\mu_{\mathrm{g,C}}(\mathrm{Kn})$. Importantly, the actual gas viscosity μ_{g} remains independent of p_0.

MODELING GAS KINETIC EFFECTS: FLOW IN A CHANNEL

Within a few mean free paths λ of gas–solid or gas–liquid surfaces there is a Knudsen layer of strong nonequilibrium flow (Hadjiconstantinou 2024) that cannot be described by the NSF formulation; in particular, the constitutive relations fail. This requires a solution of the Boltzmann equation (Cercignani 2006, Struchtrup 2005), subject to boundary conditions typically given by Maxwell's model (Maxwell 1879), that assumes diffuse scattering of a given molecule with probability α and specular reflection with probability $1-\alpha$.

Ideally, we would like to couple a solution of the Boltzmann equation in the gas with a conventional approach in the liquid. In the general case this is complex, as the Boltzmann equation requires the solution of a distribution function in unsteady six-dimensional space using methods that differ from those typically deployed on the NS equations. However, for $\mathrm{Kn} = \lambda/h \ll 1$ (in practice, $\mathrm{Kn} \lessapprox 0.1$), this layer is thin so that its influence can be attributed to boundary conditions. This apparent slip across the layer combined with actual slip at the solid is captured by a Navier slip condition. In terms of the effective viscosity, this gives $\mu_{\mathrm{g,P}} = \mu_{\mathrm{g}}/(1 + 6C\alpha\mathrm{Kn})$, where $C \approx 1$ depends on the molecular collision model used.

We have already seen that $\mathrm{Kn} > 0.1$ in many flows of interest so that the entire film must be described by the Boltzmann equation. However, applications of the lubrication approach, considered by Fukui & Kaneko (1988) for microscale gas flows between rigid solids and by Sundararajakumar & Koch (1996) and Zhang & Law (2011) for drop-based free surface flows, significantly reduce the complexity of the problem. These authors showed that the conventional lubrication approach can simply be modified by kinetic factors that account for differences in the mass flow rate and shear stress obtained from the NSF solution versus that of the Boltzmann equation. For a channel with a moving upper surface and a given pressure gradient, the problem then reduces to finding the mass flow rate Q_r and the shear stress τ_{g} on the upper surface from the Couette and Poiseuille components (plug flow is unaffected).

Wrapping the kinetic factors in effective viscosities gives an intuitive picture of how flow differs at larger Kn. A variety of approaches have been used to find these viscosities, as reviewed by Sharipov & Seleznev (1998), and they can now be rapidly obtained using numerical methods ranging from polynomial expansions (Siewert 2003) to direct simulation Monte Carlo methods (Bird 1994). Chubynsky et al. (2020) used data from solutions to the Boltzmann equation to provide formulae, and for $\alpha = 1$ (see **Figure 4*b***) these are given by

$$\mu_{\mathrm{g,P}} = \frac{\mu_{\mathrm{g}}}{1 + 6.88\mathrm{Kn} + (6\mathrm{Kn}/\pi)\log(1 + 2.76\mathrm{Kn} + 0.127\mathrm{Kn}^2)}, \qquad \text{SB1a.}$$

$$\mu_{\mathrm{g,C}} = \frac{\mu_{\mathrm{g}}}{1 + 2\mathrm{Kn}(1.1466 - 0.095\exp(-0.662/\mathrm{Kn}) - 0.0516\exp(-3.3003/\mathrm{Kn}))}. \qquad \text{SB1b.}$$

Notably, it was ensured that the correct behavior is retained in the asymptotic limits of Kn, where analytic results are available—as can be seen in Equation SB1a, the slip expression is recovered as $\mathrm{Kn} \to 0$ (with $C = 1.1466$). The accuracy of these expressions is important, as transitions can be relatively sensitive to their precise form (as they would be to changes in actual gas viscosity).

Several extensions to this simplest approach are possible and of interest (see the Future Issues section).

To include GKE, we leave mass conservation in the film unchanged (Equation 1a), but now generalize the mass flux (Equation 1b) and shear stress (Equation 2) to give

$$Q_r = \frac{-h^3}{12\mu_{\mathrm{g,P}}}\frac{\partial p_{\mathrm{g}}}{\partial r} + fhU_r/2, \qquad 5\text{a.}$$

$$\tau_{\mathrm{g}} = \frac{h}{2}\frac{\partial p_{\mathrm{g}}}{\partial r} + (2-f)\frac{\mu_{\mathrm{g,C}}U_r}{h}. \qquad 5\text{b.}$$

For the conventional model, we have $\mu_{\mathrm{g,P}} = \mu_{\mathrm{g,C}} = \mu_{\mathrm{g}}$, and there is no link to the ambient gas pressure. In contrast, with GKE firing, larger Kn reduces the effective viscosities in the film

(see **Figure 4*b***), allowing gas to escape more easily, promoting contact and thus reducing the critical We_l predicted. Notably, this can be achieved by increasing the mean free path,

$$\lambda = \frac{\lambda_{atm} p_{atm}}{p_0}, \qquad 6.$$

by either (*a*) reducing p_0 or (*b*) increasing λ_{atm} by changing the gas type—for example, it is almost three times larger in helium than in nitrogen/air. Therefore, this model has the potential to describe the observations from Section 2.

4.3. Compressibility

The assumption of incompressibility requires that changes in the density of the fluid are negligible compared to the reference value. For the liquid, this requires the Mach number to be small, as we will assume, although this can be violated (see Lesser & Field 1983, Rein 1993). A more questionable assumption is that the gas flow is incompressible.

For rigid sphere collisions in a gas, either GKE or compressibility can overcome an inadequacy of the conventional model and permit contact (Gopinath et al. 1997).

When the interface is deformable, and can respond to high pressures, both experiments (de Ruiter et al. 2012) and simulations (Chubynsky et al. 2020) for drop bouncing suggest that incompressibility is reasonable in the gas. This is supported by estimates for the maximum excess pressure by Mandre et al. (2009) and Hicks & Purvis (2011), both showing that incompressibility should hold for a millimeter-sized drop of standard liquid impacting up to 1 m/s, as confirmed in experiments by Zhang et al. (2021a). Furthermore, compressibility alone seems insufficient to allow for contact when interfaces can deform and surface tension is included (Mandre et al. 2009, Mani et al. 2010). However, it is likely that in certain regimes compressibility will come into play (for example, for higher impact speeds), and here the models proposed by Mandre et al. (2009), for a barotropic gas, or by Hicks & Purvis (2013), who consider a full analysis of the energy equation, can be implemented.

4.4. Gas Inertia

One possible link between the ambient pressure and the model is via inertial effects in the gas, which are traditionally neglected in lubrication models, but whose terms have been included by Mani et al. (2010) and Hicks & Purvis (2013), and later shown to be negligible. In contrast, without making the lubrication assumption, Jian et al. (2018) showed small corrections to bubble entrapment caused by inertia, and this deserves further attention.

4.5. Thermal Fluctuations

The reason that bouncing was observed in drop–drop collisions well before drop–solid ones is that the surfaces of droplets are typically remarkably smooth, varying only due to thermal fluctuations driving thermal capillary waves on the characteristic scale of $\ell_T = \sqrt{k_B T/\gamma}$, where k_B is Boltzmann's constant and T is the system's temperature (Aarts et al. 2004). For typical conditions, ℓ_T is of the order of nanometers so that disjoining pressure is relevant well before this scale is reached, although it is likely that the fluctuations generate the initial perturbation, as seen for thin films on solids (Fetzer et al. 2007).

4.6. Qualitative Description of the Transitions

Based on the extra physics introduced, an attractive argument for the transitions observed in drop–drop collisions, following that presented by Zhang & Law (2011), is as follows: (*a*) (regime I,

merging) at low We_l the drops remain spherical for a significant period, producing a relatively weak lubrication force so that the interfaces converge into the range at which vdW forces can pull them together; (*b*) (regime II, bouncing) at intermediate We_l, drops deform and a stronger flattened interface lubrication force keeps the interfaces out of the vdW range; and (*c*) (regime III, merging) at higher We_l, the inertia of the drops is sufficient to overcome the stronger lubrication force and push the drops back into the vdW range.

Here, GKE reduce the lubrication force so that drops can merge more easily, an effect that is enhanced at reduced ambient pressures. For drop-on-solid cases gravity is likely to play a role in the soft (I to II) transition and is not accounted for in these arguments.

5. COMPUTATIONAL MODELING

The problem considered requires the solution of the axisymmetric NS equations within the droplet whose boundary conditions are provided by a surface differential equation on a deforming interface. Consequently, several simpler modeling approaches have been considered and are discussed here. Notably, the viscosity of the gas is always included so that inviscid–inviscid balances are not considered.

Solving two-phase free boundary problems, even in three dimensions, is now a relatively routine task when all length scales and timescales within the problem are commensurate (Tryggvason et al. 2001, Popinet 2018). However, commonly drops on the scale of millimeters are dominated by lubrication forces in the gas whose thickness could be on the nanoscale—a scale separation of 10^6. Clearly, having mesh components (nodes, cells, or elements) spanning this range is impossible when the mesh is uniform and incredibly challenging when it is not, even in axisymmetric cases, let alone in fully 3D scenarios.

5.1. Weakly Deformable or Prescribed-Shape Theories

A step beyond the consideration of rigid spheres is to assume either (*a*) that deviations from the equilibrium shape are small (e.g., as in Gopinath & Koch 2002), allowing an expansion of the shape in suitable (Legendre for the axisymmetric drop) modes, or (*b*) that the shape can be defined by a few geometric parameters, as in Zhang & Law (2011), where a truncated sphere of evolving radius is used. In the former case (*a*), it is often assumed that the drop is governed by potential flow and the gas by viscous lubrication; agreement with experiments seems reasonable for $We_l \lessapprox 0.1$ (Gopinath & Koch 2002) and could or should now be validated by new simulation capabilities. These impressive articles are stepping stones toward the fully deformable case and can predict many key features.

Gopinath & Koch (2002) discovered the formation of a dimple between colliding droplets that can entrap a bubble, which is a common theme in drop–solid impacts but more difficult to observe in drop–drop cases. However, such bubbles were seen by Wang et al. (2003), where they acted as nucleation sites for internal superheating microexplosions.

Similarly, despite many simplifying assumptions (the film was assumed to be flat, viscous dissipation was approximated, etc.), the inclusion of GKE and vdW forces allowed Zhang & Law (2011) to describe qualitative features of experiments (although the quantitative values were off), such as the merge–bounce–merge transitions.

For drop impact on baths, attempts to incorporate liquid viscous dissipation have led to quasi-potential models (Dias et al. 2008) for drop bouncing (Galeano-Rios et al. 2017, Alventosa et al. 2023); extending these to consider the gas dynamics would be of interest.

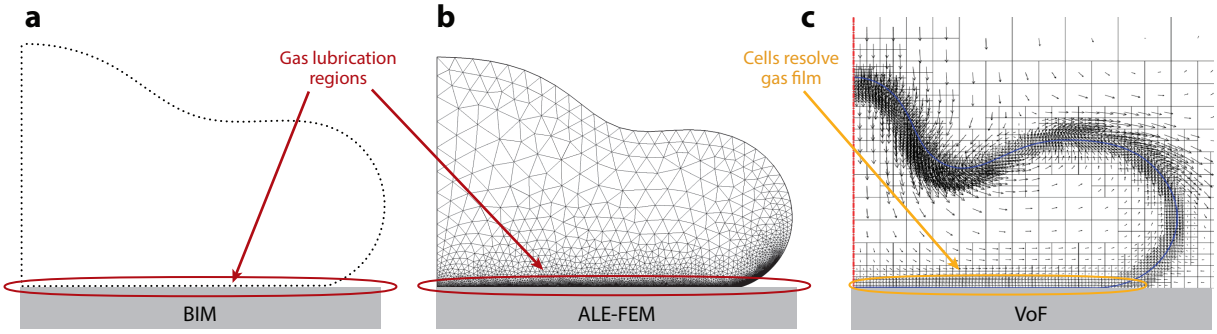

Figure 5

Hierarchy of computational modeling approaches: (*a*) boundary integral method (BIM) for an inviscid liquid, with gas lubrication; (*b*) arbitrary Lagrangian–Eulerian finite-element method (ALE-FEM) for a viscous liquid with gas lubrication; and (*c*) computation of both phases using the volume of fluid (VoF) method. Panel *b* adapted from Chubynsky et al. (2020) (CC BY 4.0). Panel *c* adapted with permission from Sharma & Dixit (2021).

5.2. Inviscid Liquid: Viscous Gas Lubrication

A popular class of models consider the liquid flow to be inviscid, with potential flow assumed, and the gas flow to be governed by lubrication; this allows one to solve a spatially 1D problem for the interface shape, for example, using the boundary integral method (see **Figure 5*a***). These models build on the work of Smith et al. (2003), who neglected surface tension, and have often focused on the bubble entrapped under an impacting droplet. Early work considered the dynamics local to the impact position, in both 2D (Mandre et al. 2009) and 3D (Hicks & Purvis 2010) configurations, while extensions to the full drop were considered by Duchemin & Josserand (2011).

A key result of this work, for both drop–drop collisions (Smith et al. 2003, Hicks & Purvis 2011) and drop–solid impacts (Duchemin & Josserand 2011), is to show that when surface tension is neglected, a corner in the free surface develops that is able to puncture the gas film and establish contact, whereas, when it is included (as in, e.g., Mandre et al. 2009), the conventional model predicts that drops will skate indefinitely on the gas. In the future, it would be interesting to focus these models on the drop bouncing phenomenon, including GKE and vdW forces to enable touchdown. However, experiments on drop bouncing typically show that altering the viscosity of either the liquid or the gas affects the transitions, so that an inviscid assumption in either is usually not possible.

5.3. Navier–Stokes in Both Phases (No Lubrication)

Once full deformation of the droplet is considered and the liquid flow is governed by the NS equations, the interior flow must be solved for using one of an array of possible methods. These can be divided into schemes in which nodes lie on the interface, such as arbitrary Lagrangian–Eulerian methods that exploit finite elements (ALE-FEM) (see Anthony et al. 2023), and those in which they do not, as in Eulerian schemes such as volume of fluid (VoF) methods (see Popinet 2018). For two-phase flow problems, VoF-type approaches are more popular, and conceptually simpler, as cells are just placed across the entire domain, including the gas film (see **Figure 5*c***).

Over the last 50 years since Foote (1975), simulations have routinely shown that numerical methods based on the conventional incompressible NS equations in the bulk can reproduce experimental behavior if the outcome of the collision event is imposed (Nobari & Tryggvason 1996, Pan et al. 2008, He et al. 2019, Liu & Bothe 2019)—i.e., a rupture time and position is chosen. For example, Pan et al. (2008) used experiments to prescribe transitions in simulations, with the

sensitivity of results to this choice shown. These authors understood that "some essential physics is missing in the simulation" (p. 9) and that vdW forces alone were insufficient—to describe the experiments GKE are also required. Similarly, Nobari & Tryggvason (1996) noted that the "principle weakness of the simulations presented here is the ad-hoc way the film between the drops is ruptured for coalescing drops" (p. 755).

For drop–solid impacts, the gas phase has often been neglected (Fukai et al. 1995), with success at describing some features, while including it results in the formation of gas bubbles (Josserand & Zaleski 2003, Fu et al. 2021). Recent progress was presented in an interesting article by Sharma & Dixit (2021), who considered a VoF approach with mesh resolutions that reach ∼1 μm for the impact of a millimeter-sized droplet. Their results were based on the conventional model, but they nevertheless captured many experimental trends and were able to validate several proposed scaling laws for the process. As there is no physical mechanism to induce rupture in their model, the criterion for contact is that the film height goes below the resolution of the mesh—with further resolution one may expect bouncing to occur in all cases. Notably, their resolution was of the same magnitude as the heights at which de Ruiter et al. (2015b,c) saw film collapse, and this may explain why there is slightly better agreement with these experiments than those of Kolinski et al. (2014).

Similar techniques, with consistent conclusions to those above, have been used to consider drop impact on baths/films (Josserand & Zaleski 2003, Pan & Law 2007, Alventosa et al. 2023), including using different liquids for the bath and drop (Fudge et al. 2021).

A breakthrough came from Li (2016). For a fully deformable drop, this was the first computational model to incorporate vdW and GKE, exploiting an effective viscosity approach, using ALE-FEM within the liquid and gas phase in a highly spatially adaptive manner—with five orders of magnitude just to capture the film with a single layer of elements. Shapes for drop bouncing agreed with those from Pan et al. (2008), but the real advance was the quantitative prediction of transitions between merging and bouncing from the experiments of Qian & Law (1997), notably, recovering the effects of ambient gas pressure via GKE and demonstrating dependencies on drop viscosity, which elude the models of Section 5.2.

The disadvantage of this class of models is the huge computational cost associated with resolving (i.e., meshing) the gas film alongside the drop.

5.4. Navier–Stokes Liquid: Viscous Gas Lubrication

To overcome the multiscale burden associated with the models of Section 5.3, Chubynsky et al. (2020) developed a computational model similar to that of Li (2016), including GKE and vdW in an ALE-FEM framework (see **Figure 5*b***), but with the gas dynamics manifesting as a boundary condition for the liquid's flow, through the lubrication approach, in keeping with the philosophy of Section 5.2.

5.4.1. Drop–solid modeling. The focus of Chubynsky et al. (2020) was drop bouncing on solid surfaces. From a modeling perspective, this requires a second effective viscosity, associated with Couette flow, which cannot fit into the approach of Li (2016). It is this component that Lo et al. (2017) showed is crucial to predicting drop bouncing transitions.

Chubynsky et al. (2020) were able to reproduce the transition between bouncing and merging observed by Kolinski et al. (2014), with the numerical threshold at $We_l = 7.4$, compared to $We_l = 7.6$ experimentally. GKE were shown to be crucial to predicting transitions: Neglecting GKE (but keeping vdW forces) moves the Weber number to $We_l > 16$ and probably as high as ≈50 (for details, see Chubynsky et al. 2020) (see **Figure 6*c***), while neglecting vdW forces leads to rebound in all cases. Notably, vdW forces bring fascinating additional effects that manifest themselves most strongly in the film mode, with vdW-driven surface waves seen to grow and induce

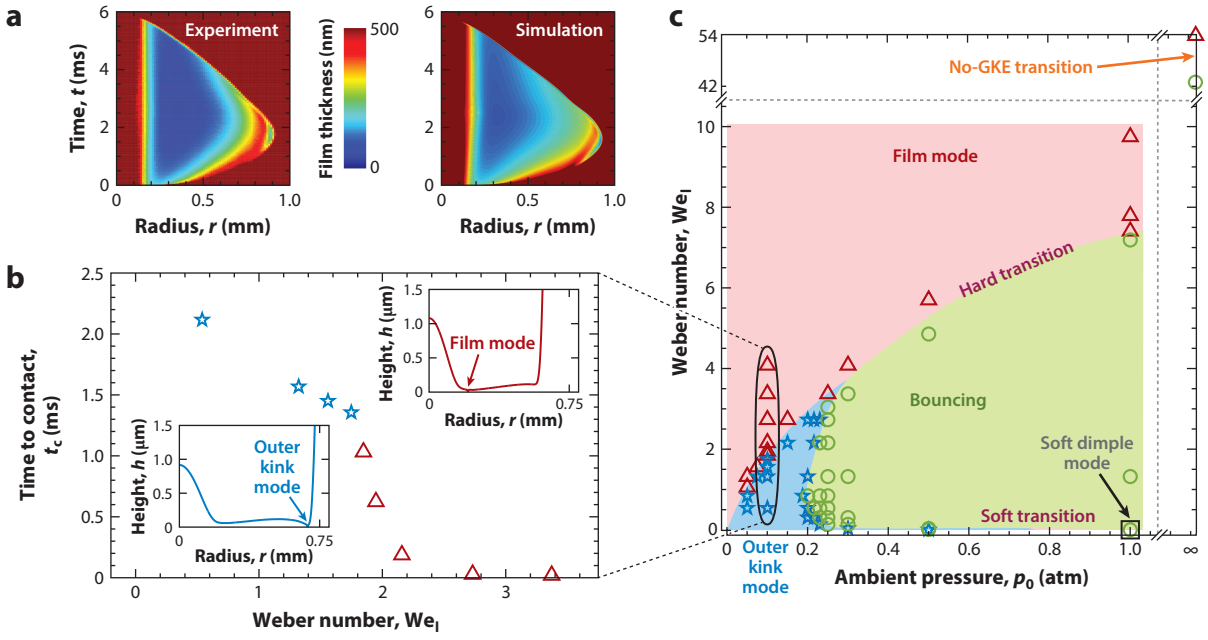

Figure 6

Computations from Chubynsky et al. (2020) for water-glycerol drops of radius $R = 0.8$ mm and viscosity $\mu_l = 11.55$ mPa · s showing (*a*) qualitative agreement with the experiments of Kolinski et al. (2014) for film height evolution at Weber number $We_l = 4.1$ (though with a difference in absolute height, as discussed in the text); (*b*) identification of short and long times-to-contact with, respectively, film and outer kink contact modes (*insets*); and (*c*) a regime diagram identifying modes of contact [see Chubynsky et al. (2020) for more details on the location of the no-GKE (gas kinetic effects) transition]. Figure adapted from Chubynsky et al. (2020) (CC BY 4.0).

contact. The linear stability theory in Chubynsky et al. (2020) predicts the growth rate. An interesting question is what to choose as the initial perturbation for these waves, with Chubynsky et al. (2020) attributing this to thermal fluctuations, even though in computations, at present, it is numerical noise that triggers the instability. Clearly, this issue deserves further attention.

5.4.2. Drop–solid film heights. **Figure 6*a*** shows that excellent qualitative agreement was obtained with Kolinski et al. (2014) for the film profiles, with both a dimple on the axis and an outer kink near the edge reproduced (see also the comparison at **https://youtu.be/YX8ChCLhBoo**). However, Chubynsky et al. (2020) showed the film heights close to the transition are around 20 nm, compared to ≈2 nm reported by Kolinski et al. (2014) and ≈200 nm by de Ruiter et al. (2015b,c). The likely reason for the discrepancy with Kolinski et al. (2014) is a bias in the experimental TIR method used, as described by Shirota et al. (2017), and this is supported by more recent experiments (Kaviani & Kolinski 2023). In contrast, the larger heights from de Ruiter et al. (2015b) initially suggest the presence of isolated asperities in the solid, on an otherwise nanometrically smooth surface, puncturing the air film and prematurely inducing contact, with Kolinski et al. (2014) noting that bouncing is repeatable for impact onto freshly cleaved mica but sporadic for cleaned glass and silicon substrates. However, similar heights for film collapse are reported by Zhang et al. (2021a), where an oil film is used to mask asperities, making the picture rather murkier and suggesting that additional effects, such as the electrostatic interactions suggested by de Ruiter et al. (2015c), should be considered.

5.4.3. Drop–solid contact modes. Chubynsky et al. (2020) predicted three modes of contact: the film and kink modes already seen (**Figure 6*b***), as well as a mode in which contact occurs at the drop axis just before the liftoff. However, in contrast to the mode described by Zhang et al. (2021a), this one exists at very low impact speeds, is not dependent on the liquid having low viscosity, and is a soft transition—we call it a soft dimple mode.

Virtual experiments conducted by Chubynsky et al. (2020) showed the strong influence of p_0 on transitions, created by GKE, with no bouncing seen below a critical value, as commonly reported in experiments. Also shown (see **Figure 6*b***) was that the time-to-contact can often be used as a signature of the contact mode, with the film mode associated with an earlier contact than the outer kink mode. Whilst an entrapped bubble was predicted in certain cases, ALE-FEM is not well suited to going through topological transitions, so the influence of this on the dimple mode of contact remained unexplored (for simulations in which it is captured, see Sharma & Dixit 2021).

Interestingly, for water-glycerol drops with $\mu_l \approx 10$ mPa · s, the transition seen by Zhang et al. (2021a) is at a lower We_l than that seen for the same parameters by both Chubynsky et al. (2020) and Kolinski et al. (2014). The reason for this discrepancy is unknown, as the film coating used by Zhang et al. (2021a) was assumed to act as a rigid undeformable surface.

5.5. Open-Source Computational Framework for Navier–Stokes Liquid with Gas Lubrication

The success of the computational model developed in Chubynsky et al. (2020) has motivated us to develop and release an open-source version of this code, available at **https://github.com/PLewinJones/drop_impact**, in the superb finite element library oomph-lib (Heil et al. 2022), for both drop–drop and drop–solid cases. This code produced the outlines in **Figure 1**, and scripts are provided for users to reproduce these cases.

We take this opportunity to revisit drop–drop collisions with our new framework, which allows us to compare to experimental data from Qian & Law (1997) and Huang & Pan (2021) for droplets of tetradecane of radius $R \approx 150$ μm ($\rho_l = 762$ kg/m^3, $\mu_l = 2.13$ mPa · s, $\mu_g = 1.84 \times 10^{-2}$ mPa · s, $\gamma = 26.5$ mN/m, $A = 5 \times 10^{-20}$ J) at different impact speeds, with a focus on the influence of ambient pressure and gas type. In particular, the inset of **Figure 7*b*** shows that we are able to capture the experimental transitions relatively well, in both nitrogen and helium, with the exception of a single nitrogen data point, an outlier that we believe is due to experimental inaccuracies. Furthermore, in contrast to the experiments, we can access the film profiles at merging, as shown in **Figure 7*a***. There, we can see the film (contact near the inner kink, at an early time) and outer kink modes previously described, but also a late film mode during which the drop spends significant time spreading out before contact is initiated at a point between the inner and outer kinks.

To more quantitatively establish a regime diagram, we contour plot the time-to-contact t_c and radius r_c (normalized by characteristic scales $T_i = \sqrt{\rho_l R^3/\gamma}$ and R, respectively) of all the contacts, as shown in **Figure 7*b*,*c***. The transition between early film and outer kink/late-film modes can be clearly seen in **Figure 7*c*** and is highlighted by a dashed line. In contrast, no clear demarcation can be made between outer kink and late-film modes. In this region, the outcome is quite sensitive to parameters—as one can see from **Figure 7*a***, where vdW-driven waves are growing in different regions and competing to complete merging. Notably, the regime diagram looks quite different from those already shown for drop–solid collisions, and it remains to be established if this is because the processes are different or if it is simply due to the different parameter regime.

Soft transitions are also seen and a typical profile for contact is shown in the inset of **Figure 7*c***. Contact occurs during the rebound phase (centers of mass moving apart) at the only kink; therefore, this mode is associated with a large t_c (see **Figure 7*b***).

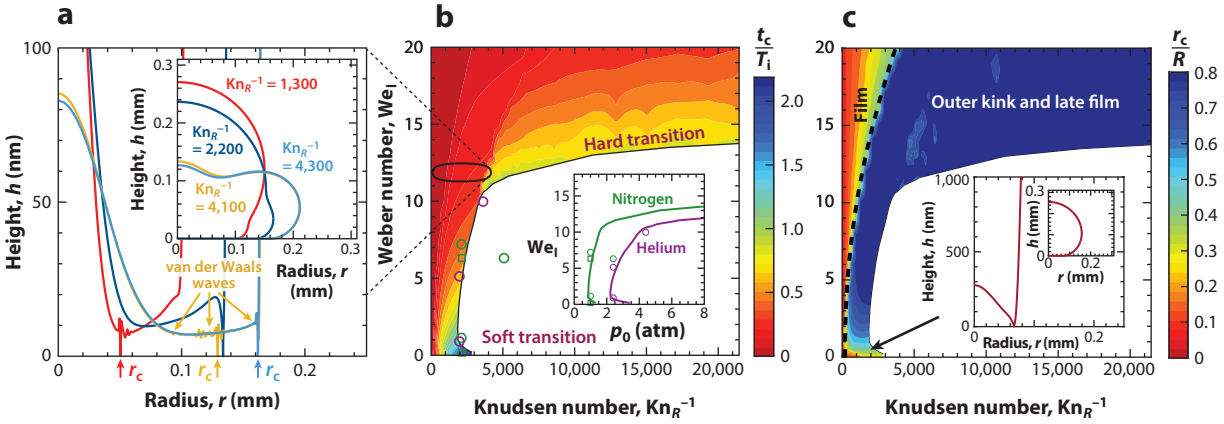

Figure 7

Comparison of computations and experiments for tetradecane droplets of radius $R = 150$ μm. (*a*) Computed profiles of droplets merging in different modes. Their positions on the regime diagram are shown. (*b*) (*Inset*) Comparison of computations (*solid lines*) with experimental data from Huang & Pan (2021) (*squares*) and Qian & Law (1997) (*circles*) for the transition between bouncing and merging in nitrogen and helium, as ambient pressure p_0 is varied. The main plot shows the collapse of simulation data and experiments when using the Knudsen number $Kn_R = \lambda/R$ as a dimensionless coordinate, with a mean free path $\lambda_{atm} = 69$ nm for nitrogen and $\lambda_{atm} = 184$ nm for helium. Contours show the time-to-contact t_c, normalized by the inertial timescale $T_i = \sqrt{\rho_l R^3/\gamma}$. The white region corresponds to bouncing. (*c*) (*Inset*) Computed profile for a soft transition, which merges during rebound. The main plot shows contours for the radial position of contact r_c, normalized by the droplet size R.

Figure 7*b* shows that the experimental data for the two gases can be collapsed onto a single transition curve if we use the Knudsen number based on drop size $Kn_R = \lambda/R$ as a dimensionless coordinate, using Equation 6 to find $\lambda(p_0)$. In other words, introducing GKE has allowed us to understand how the gas type shifts the transitions. In future, it would be interesting to attempt to go one step further and choose our macroscopic length scale based on the predicted minimum film height in an attempt to collapse data for different liquids too, for example, using the models of Mandre et al. (2009) or Huang & Pan (2021).

6. LEIDENFROST LEVITATION AND BOUNCING

When liquid drops are gently deposited onto a hot solid surface, above a critical temperature the lifetime of the drop abruptly increases (Biance et al. 2003) due to the so-called Leidenfrost effect, with the drop levitating on its own vapor layer and thus thermally shielded from the hot solid; this effect is reviewed by Quéré (2013). The quasi-static equilibrium state is now relatively well understood, with experiments for the film profile (Biance et al. 2003, Burton et al. 2012) aligning with theory (Sobac et al. 2014) and computation (Chakraborty et al. 2022), when the flow remains axisymmetric.

Recent experiments have focused on understanding behavior around the Leidenfrost temperature, with two separate values being identified: a high temperature for the formation of a vapor layer T_L^+ from a wetted state and a lower one T_L^- for collapse of the vapor layer, with an intermediate metastable regime. Beautiful experiments by Harvey et al. (2021) show this cycle (see their supplemental video 3), and Chantelot & Lohse (2021b) have interpreted the metastable regime in the framework of directed percolation in order to provide a new method for defining T_L^+. The physics underlying the vapor collapse and, hence, T_L^- are fascinating, remain unclear, and deserve further attention. For example, a stability analysis conducted by Aursand et al. (2018) claims thermocapillarity (aided by GKE) is the main destabilizing mechanism, Zhao & Patankar (2020)

posited that vdW forces are the dominant physics, and recent work by Harvey & Burton (2023) points to a hydrodynamic inertia-driven instability.

6.1. The Dynamic Leidenfrost Effect

A dynamic Leidenfrost effect (Tran et al. 2012, Staat et al. 2015, Shirota et al. 2016, Lee et al. 2020) is encountered when droplets impacting a hot surface are able to avoid contact by producing a strong vapor/gas cushion. This is a combination of drop bouncing and levitation, with recent experiments showing that both the ambient gas and the vapor generated from the evaporating droplet play a role in the drop's dynamics (Chantelot & Lohse 2021a). Full simulations of the dynamic Leidenfrost phenomenon, which could test the assumptions of recent theories, such as Gordillo & Riboux (2022), remain incomplete.

6.1.1. Phenomenology of the film and modes of touchdown. Leidenfrost impacts studied by Chantelot & Lohse (2021a) showed features similar to their isothermal counterparts, particularly in the initial stages where a dimple forms and the ambient gas dynamics appear more important than the vapor's. In contrast, as the drop spreads over a vapor film, the inner kink's position becomes dynamic (being driven upward), unlike the isothermal case, so that the film thickness now depends on the evaporation.

Two main modes of contact were reported by Chantelot & Lohse (2021a) for the hard transition: a short-time film mode contact (see **Figure 8*a***) and a later-time dimple mode (**Figure 8*b***) associated with contact at the film's center during rebound. However, there is a region of parameter space, spanning both contacts and bouncing, where the authors observed a novel mode in which the gas film oscillates (see **Figure 8*c***). As with the isothermal case, capillary waves for low-viscosity liquids generate complex behavior (see **Figure 8*b***) that can cause dimple mode touchdown.

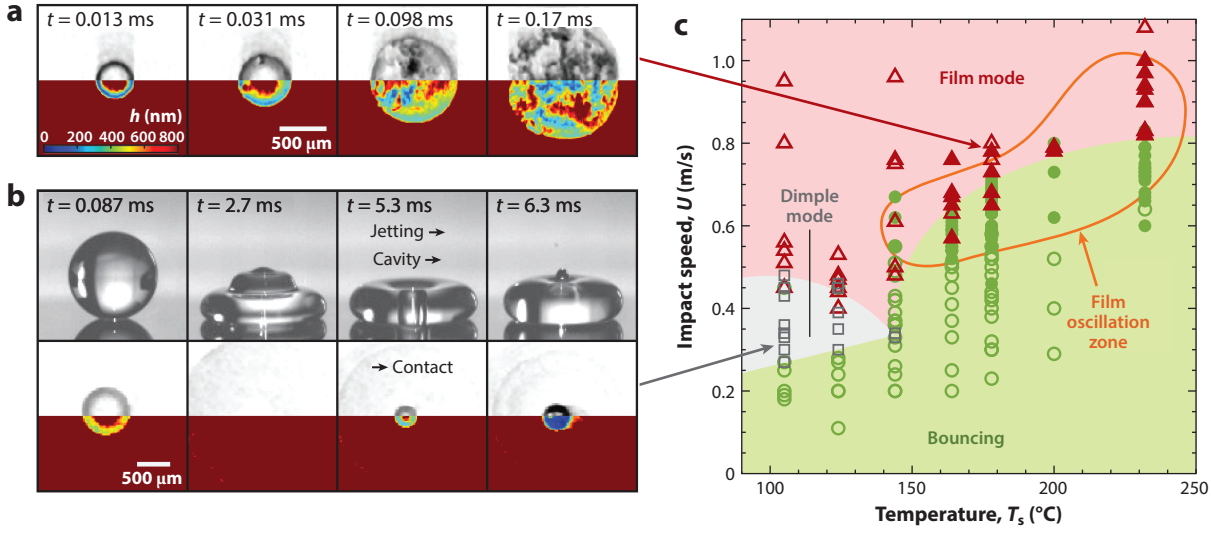

Figure 8

Experimental results by Chantelot & Lohse (2021a) showing total internal reflection images for (*a*) a film mode and (*b*) a dimple mode of contact, alongside side-on images showing how the latter coincides with jetting and air cavity formation. (*c*) A regime diagram across impact speed U (material parameters vary with temperature, so the Weber number We_l is less easily defined) and substrate temperature T_s for ethanol drops. Filled symbols indicate experiments in which gas film oscillations were observed. Arrows indicate the position of panels *a* and *b* on the regime diagram. Figure adapted from Chantelot & Lohse (2021a) (CC BY 4.0).

6.1.2. Pressure dependence. Interestingly, the Leidenfrost temperature depends on p_0 for the quasi-static case, but this can be attributed to the thermodynamics (van Limbeek et al. 2021). The dynamic Leidenfrost temperature also depends on ambient pressure (van Limbeek et al. 2018), and the picture there is less clear and deserves further attention, with lower pressures leading to an unexplained increased dependence of T_L on impact speed.

q_v: heat flux in the vapor normal to the solid

k_v: thermal conductivity of the vapor

T_s: temperature of the solid

T_l: temperature of the liquid

j: mass flux from the liquid

L: latent heat of evaporation

ρ_v: density of the vapor

6.2. Modeling the Leidenfrost Effect: Statics and Dynamics

Sobac et al. (2014) proposed a model to calculate the shapes of axisymmetric quasi-static Leidenfrost droplets that matches an evaporation-driven viscous lubrication description of the film to a Young–Laplace-type model for the upper surface of the droplet. In this model, it is assumed that heat transfer in the gas is dominated by conduction so that the temperature varies linearly between the solid, which has a fixed temperature (for extensions, see van Limbeek et al. 2017), and the drop (assumed to be at the boiling temperature). Then, the heat flux into the drop, $q_v = k_v(T_s - T_l)/h$, is balanced by the loss of energy through evaporation, so that $j = q_v/L$. The layer is assumed to only be composed of vapor. Predictions for the film's shape are generally in excellent agreement with experiments, showing that for static droplets these assumptions appear reasonable.

To go beyond the quasi-static case, Chakraborty et al. (2022) considered an extension of the models of Sobac et al. (2014), for the evaporation, and Chubynsky et al. (2020), for the dynamics, in balancing a Navier–Stokes description in the liquid with a lubrication approach in the film. The evaporative flux into the film requires the conservation of mass Equation 1a to be generalized, to give

$$\frac{\partial h}{\partial t} + \frac{1}{r}\frac{\partial (rQ_r)}{\partial r} = \frac{k_v(T_s - T_l)}{\rho_v h L}, \qquad 7.$$

and as a first step, there is no GKE or vdW so that the flux is given by Equation 1b and stress by Equation 2. The Sobac et al. model can be recovered for the film by considering an equilibrium state, $\partial h/\partial t = 0$ in Equation 7; neglecting internal flow, so that $U_r = 0$ in Equation 1b; and thus not requiring τ_g.

The model of Chakraborty et al. (2022) shows good agreement with that of Sobac et al. and, therefore, experiments when internal flow is neglected. Furthermore, it can capture the dynamics of the chimney instability, in which the vapor film punctures the center of the drop, and could be extended to study dynamic Leidenfrost cases. Interestingly, however, when internal flow is included in the computational model, this flow drives larger water drops to transition into new shapes not seen experimentally; as discussed by Chakraborty et al. (2022), this is likely due to symmetry-breaking in the experiments (see Section 7.2).

7. SOME RELATED TOPICS

Supplemental Material >

Thin films of gas influence the dynamics of free surface flows in an array of other configurations, and a few are briefly considered here; readers are referred to **Supplemental Appendix B**: Details of Future Issues for more.

7.1. Permanent Noncoalescence

If two liquid–gas interfaces are moving tangentially to each other (i.e., axisymmetry is lost), air can be dragged into the lubrication region between them to prevent contact and, in certain cases, create a stable levitated equilibrium state. This can occur, for example, by moving an underlying liquid surface (Pirat et al. 2010, Castrejón-Pita et al. 2016, Gauthier et al. 2016) or by mobilizing

the droplet, for example, to run downhill (Law & Chu 2019). Alternatively, flow can be (axisymmetrically) induced into the film through the thermal Marangoni surface force (see Neitzel & Dell'Aversana 2002).

7.2. Symmetry-Breaking

Off-center collisions and oblique impacts lead to a loss of axisymmetry and an additional parameter associated with the angle of approach is needed in the model. However, even in initially axisymmetric cases, contact usually occurs at a point away from the drop center to kill the symmetry. Particularly surprising are the experimental results of Lo et al. (2017) for the soft transition, showing that rapid symmetry-breaking only requires small surface tilts [see video 1 of the multimedia from Lo et al. (2017)].

For Leidenfrost cases, larger puddle-like drops often break their symmetry due to the self-excitation of droplet wave modes (Brunet & Snoeijer 2011, Ma et al. 2017, Bouillant et al. 2021). However, more recently, smaller Leidenfrost wheel droplets were observed by Bouillant et al. (2018) to also spontaneously break symmetry (see **https://youtu.be/glRGl-eYuXo**)—leading to rapid droplet motion in a random direction. Similar breaking of axisymmetry was seen by Yim et al. (2022) in the creation of internal cells for larger droplets [see supplemental movie 1 from Yim et al. (2022)]. Theory for the wheels from Brandão & Schnitzer (2020) and computation of the cells from Yim et al. (2022) have provided important insight into these mechanisms.

7.3. Trampolining

The picture of Leidenfrost droplets coming to rest in a static state has recently been shattered by observations in Liu & Tran (2020) and Graeber et al. (2021) of spontaneous droplet trampolining [see **Figure 9*c*** and supplemental movie 1 from Graeber et al. (2021)]. Similarly, evaporation can drive hydrogel spheres to perform self-sustained bouncing on hot surfaces (see Waitukaitis et al. 2017 and **https://youtu.be/vPSZYHaDUqI**); models developed here could be extended to describe this, now using elasticity in the drop (see Binysh et al. 2022).

7.4. Dynamic Wetting

For drops impacting solids at higher speeds, one is often interested in whether they splash, with a particular interest in how the ambient gas affects this process (see **Figure 9*a***). It is now well recognized that the entrapped bubble is far from where splashing occurs (Driscoll & Nagel 2011, Liu et al. 2015, Josserand & Thoroddsen 2016) so that to describe the effects of gas pressure and type on splashing, a dynamic wetting process must be considered. The question then is how fast a liquid can travel across (i.e., wet) a given solid before wetting failure occurs (Blake & Ruschak 1979, Rein & Delplanque 2008, Vandre et al. 2012), corresponding here to the lamella detaching from the substrate and remaining airborne.

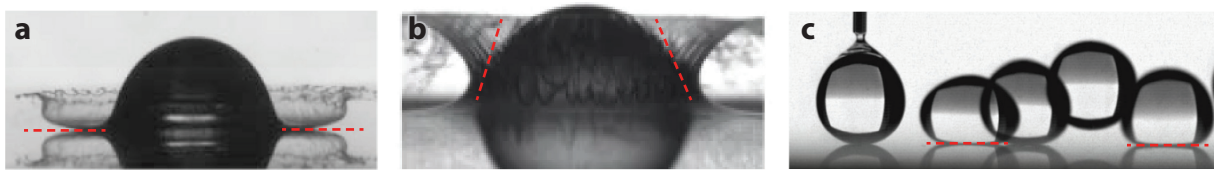

Figure 9

Gas microfilms (*red dashed lines*) in (*a*) a splashing droplet, (*b*) a solid sphere impacting an interface, and (*c*) a droplet trampolining on a hot surface. Panels adapted from (*a*) Xu et al. (2005) (CC BY 4.0); (*b*) Duez et al. (2007) (with permission); and (*c*) Graeber et al. (2021) (CC BY 4.0).

This is the picture proposed in the theory of Riboux & Gordillo (2014), where the influence of GKE in the gas film, included via slip conditions by Gordillo & Riboux (2019), is crucial to describing experimental data of Xu et al. (2005) and Hao et al. (2019). There are many similarities here to coating flows, where air entrainment is typically the enemy of the industrialist, as explored by Marchand et al. (2012; see the movie in the supplemental material); Sprittles (2017), where GKE were used to describe coating experiments conducted at reduced pressures (Benkreira & Khan 2008); and Sprittles (2015), where experimental data for splashing transitions were collapsed using GKE. Interestingly, experiments by Usawa et al. (2021) showed that for smaller microdrops, splashing is less likely for a given We_l, as the flow dimensions become closer to the mean free path in the gas so that the lubrication force is reduced. The model developed here could capture this effect.

The interplay of dynamic wetting and gas films also underpins the relation between precontact and postcontact dynamics, explored by Zhang et al. (2022) and by de Goede et al. (2019) under different ambient conditions; the entrapment of gas bubbles during spreading (Thoroddsen et al. 2010); the remarkable extreme wetting of liquid bridges that have formed in drop contact spots (Langley et al. 2017); the influence of gas on cavity formation when solid spheres impact baths (see **Figure 9*b***) (Duez et al. 2007, Williams et al. 2022); and the stability of wetting contacts on hot surfaces, which govern Leidenfrost stability (Chantelot & Lohse 2021b).

SUMMARY POINTS

1. Transitions between bouncing and merging rely on physics at the nanoscales to microscales, most notably, gas kinetic effects (GKE) and van der Waals forces. Once implemented into accurate computational models, experimental observations can be reproduced.
2. Accurate computational models must either (*a*) resolve the small scales in the gas or (*b*) use a lubrication model for the gas phase.
3. Sharing knowledge between drop–drop and drop–solid cases is worthwhile. Experimentally, the former case removes worries about asperities while the latter allows for resolution of the film. Mathematically the two cases are almost identical in their basic state.

FUTURE ISSUES

Supplemental Material >

We expand upon the following in **Supplemental Appendix B**: Details of Future Issues.

1. Create a computational framework that (*a*) accounts for the microphysics, (*b*) goes through topological changes, and (*c*) is tractable in 3D.
2. Extend the model, particularly for GKE, to (*a*) improve its accuracy, (*b*) account for nonisothermal cases, and (*c*) capture nonlubrication regimes.
3. Probe impacts in gas/vapor mixtures.
4. Understand how a solid's asperities or electrostatic effects contribute to touchdown in both isothermal and Leidenfrost conditions.
5. Study a far wider range of material parameters and drop sizes.

6. Tackle an array of free surface flows that are influenced by thin layers of gas and are ripe for theoretical attack.
7. Build additional physical effects on top of the basic framework.

DISCLOSURE STATEMENT

The author is not aware of any biases that might be perceived as affecting the objectivity of this review.

ACKNOWLEDGMENTS

First and foremost, the author acknowledges Mykyta Chubynsky, Duncan Lockerby, and Yulii Shikhmurzaev for the scientific knowledge they have shared with him. The new work in Section 5.5 is part of Peter Lewin-Jones' PhD thesis and will soon be published in a standalone article; the release of open-source code was only possible with his expertise. Many thanks also to those who have contributed by providing data, knowledge, or critical reading of drafts, namely: Terry Blake, Alfonso Castrejón-Pita, Pierre Chantelot, Radu Cimpeanu, Livio Gibelli, Madeleine Moore, Jolet de Ruiter, Kuo-Long Pan, Ying Sun, and Lige Zhang. The author acknowledges funding from the Leverhulme Trust and multiple EPSRC (Engineering and Physical Sciences Research Council) grants, most notably EP/W031426/1, EP/S029966/1, EP/P031684/1, and EP/N016602/1.

LITERATURE CITED

Aarts DGAL, Schmidt M, Lekkerkerker HNW. 2004. Direct visual observation of thermal capillary waves. *Science* 304(5672):847–50

Ababaei A, Rosa B. 2023. Collision efficiency of cloud droplets in quiescent air considering lubrication interactions, mobility of interfaces, and noncontinuum molecular effects. *Phys. Rev. Fluids* 8:014102

Abouelsoud M, Bai BÇ. 2021. Bouncing and coalescence dynamics during the impact of a falling drop with a sessile drop on different solid surfaces. *Phys. Fluids* 33(6):063309

Al-Dirawi KH, Bayly AE. 2019. A new model for the bouncing regime boundary in binary droplet collisions. *Phys. Fluids* 31(2):027105

Alventosa LFL, Cimpeanu R, Harris DM. 2023. Inertio-capillary rebound of a droplet impacting a fluid bath. *J. Fluid Mech.* 958:A24

Anthony CR, Wee H, Garg V, Thete SS, Kamat PM, et al. 2023. Sharp interface methods for simulation and analysis of free surface flows with singularities: breakup and coalescence. *Annu. Rev. Fluid Mech.* 55:707–47

Aursand E, Davis SH, Ytrehus T. 2018. Thermocapillary instability as a mechanism for film boiling collapse. *J. Fluid Mech.* 852:283–312

Bach GA, Koch DL, Gopinath A. 2004. Coalescence and bouncing of small aerosol droplets. *J. Fluid Mech.* 518:157–85

Benkreira H, Khan M. 2008. Air entrainment in dip coating under reduced air pressures. *Chem. Eng. Sci.* 63(2):448–59

Biance AL, Clanet C, Quéré D. 2003. Leidenfrost drops. *Phys. Fluids* 15(6):1632

Binysh J, Chakraborty I, Chubynsky MV, Melian VLD, Waitukaitis SR, et al. 2022. Thermodynamic lubrication in the elastic Leidenfrost effect. arXiv:2207.02769 [cond-mat.soft]. **https://doi.org/10.48550/arXiv.2207.02769**

Bird GA. 1994. *Molecular Gas Dynamics and the Direct Simulation of Gas Flows*. Oxford, UK: Oxford Univ. Press

Blake TD, Ruschak KJ. 1979. A maximum speed of wetting. *Nature* 282(5738):489–91

Bouillant A, Cohen C, Clanet C, Quéré D. 2021. Self-excitation of Leidenfrost drops and consequences on their stability. *PNAS* 118(26):e2021691118
Bouillant A, Mouterde T, Bourrianne P, Lagarde A, Clanet C, Quéré D. 2018. Leidenfrost wheels. *Nat. Phys.* 14(12):1188–92
Bouwhuis W, van der Veen RCA, Tran T, Keij DL, Winkels KG, et al. 2012. Maximal air bubble entrainment at liquid-drop impact. *Phys. Rev. Lett.* 109(26):264501
Brandão R, Schnitzer O. 2020. Spontaneous dynamics of two-dimensional Leidenfrost wheels. *Phys. Rev. Fluids* 5(9):091601
Brunet P, Snoeijer J. 2011. Star-drops formed by periodic excitation and on an air cushion—a short review. *Eur. Phys. J. Spec. Top.* 192:207–26
Burton JC, Sharpe AL, van der Veen RCA, Franco A, Nagel SR. 2012. Geometry of the vapor layer under a Leidenfrost drop. *Phys. Rev. Lett.* 109(7):074301
Bush JW. 2015. Pilot-wave hydrodynamics. *Annu. Rev. Fluid Mech.* 47:269–92
Castrejón-Pita JR, Muñoz-Sánchez BN, Hutchings IM, Castrejón-Pita AA. 2016. Droplet impact onto moving liquids. *J. Fluid Mech.* 809:716–25
Cercignani C. 2006. *Slow Rarefied Flows*. Basel, Switz.: Birkhäuser
Chakraborty I, Chubynsky MV, Sprittles JE. 2022. Computational modelling of Leidenfrost drops. *J. Fluid Mech.* 936:A12
Chan DYC, Klaseboer E, Manica R. 2011. Film drainage and coalescence between deformable drops and bubbles. *Soft Matter* 7(6):2235–64
Chantelot P, Lohse D. 2021a. Drop impact on superheated surfaces: short-time dynamics and transition to contact. *J. Fluid Mech.* 928:A36
Chantelot P, Lohse D. 2021b. Leidenfrost effect as a directed percolation phase transition. *Phys. Rev. Lett.* 127(12):124502
Chubynsky MV, Belousov KI, Lockerby DA, Sprittles JE. 2020. Bouncing off the walls: the influence of gas-kinetic and van der Waals effects in drop impact. *Phys. Rev. Lett.* 124(8):084501
Couder Y, Fort E, Gautier CH, Boudaoud A. 2005. From bouncing to floating: noncoalescence of drops on a fluid bath. *Phys. Rev. Lett.* 94(17):177801
Cuttle C, Thompson AB, Pihler-Puzović D, Juel A. 2021. The engulfment of aqueous droplets on perfectly wetting oil layers. *J. Fluid Mech.* 915:A66
Davis MH. 1972. Collisions of small cloud droplets: gas kinetic effects. *J. Atmos. Sci.* 29(5):911–15
Davis MH, Sartor JD. 1967. Theoretical collision efficiencies for small cloud droplets in Stokes flow. *Nature* 215(5108):1371–72
Davis RH, Schonberg JA, Rallison JM. 1989. The lubrication force between two viscous drops. *Phys. Fluids A* 1:77–81
de Goede TC, de Bruin KG, Shahidzadeh N, Bonn D. 2019. Predicting the maximum spreading of a liquid drop impacting on a solid surface: effect of surface tension and entrapped air layer. *Phys. Rev. Fluids* 4(5):053602
de Ruiter J, Lagraauw R, Mugele F, van den Ende D. 2015a. Bouncing on thin air: how squeeze forces in the air film during non-wetting droplet bouncing lead to momentum transfer and dissipation. *J. Fluid Mech.* 776:531–67
de Ruiter J, Lagraauw R, van den Ende D, Mugele F. 2015b. Wettability-independent bouncing on flat surfaces mediated by thin air films. *Nat. Phys.* 11:48–53
de Ruiter J, Oh JM, van den Ende D, Mugele F. 2012. Dynamics of collapse of air films in drop impact. *Phys. Rev. Lett.* 108(7):074505
de Ruiter J, van den Ende D, Mugele F. 2015c. Air cushioning in droplet impact. II. Experimental characterization of the air film evolution. *Phys. Fluids* 27:012105
Dias F, Dyachenko AI, Zakharov VE. 2008. Theory of weakly damped free-surface flows: a new formulation based on potential flow solutions. *Phys. Lett. A* 372(8):1297–302
Driscoll MM, Nagel SR. 2011. Ultrafast interference imaging of air in splashing dynamics. *Phys. Rev. Lett.* 107(15):154502
Duchemin L, Josserand C. 2011. Curvature singularity and film-skating during drop impact. *Phys. Fluids* 23(9):091701

Duchemin L, Josserand C. 2020. Dimple drainage before the coalescence of a droplet deposited on a smooth substrate. *PNAS* 117(34):20416–22
Duez C, Ybert C, Clanet C, Bocquet L. 2007. Making a splash with water repellency. *Nat. Phys.* 3(3):180–83
Fetzer R, Rauscher M, Seemann R, Jacobs K, Mecke K. 2007. Thermal noise influences fluid flow in thin films during spinodal dewetting. *Phys. Rev. Lett.* 99(11):114503
Foote GB. 1975. The water drop rebound problem: dynamics of collision. *J. Atmos. Sci.* 32(2):390–402
Fu Z, Jin H, Zhang J, Xue T, Wen D. 2021. Air film evolution during droplet impact onto a solid surface. *Phys. Fluids* 33(9):092107
Fudge BD, Cimpeanu R, Castrejón-Pita AA. 2021. Dipping into a new pool: the interface dynamics of drops impacting onto a different liquid. *Phys. Rev. E* 104(6):065102
Fukai J, Shiiba Y, Yamamoto T, Miyatake O, Poulikakos D, et al. 1995. Wetting effects on the spreading of a liquid droplet colliding with a flat surface: experiment and modeling. *Phys. Fluids* 7(2):236–47
Fukui S, Kaneko R. 1988. Analysis of ultra-thin gas film lubrication based on linearized Boltzmann equation: first report—derivation of a generalized lubrication equation including thermal creep flow. *J. Tribol.* 110(2):253–61
Galeano-Rios CA, Milewski PA, Vanden-Broeck JM. 2017. Non-wetting impact of a sphere onto a bath and its application to bouncing droplets. *J. Fluid Mech.* 826:97–127
Gauthier A, Bird JC, Clanet C, Quéré D. 2016. Aerodynamic Leidenfrost effect. *Phys. Rev. Fluids* 1(8):084002
Gopinath A, Chen SB, Koch DL. 1997. Lubrication flows between spherical particles colliding in a compressible non-continuum gas. *J. Fluid Mech.* 344:245–69
Gopinath A, Koch DL. 2002. Collision and rebound of small droplets in an incompressible continuum gas. *J. Fluid Mech.* 454:145–201
Gordillo JM, Riboux G. 2019. A note on the aerodynamic splashing of droplets. *J. Fluid Mech.* 871:R3
Gordillo JM, Riboux G. 2022. The initial impact of drops cushioned by an air or vapour layer with applications to the dynamic Leidenfrost regime. *J. Fluid Mech.* 941:A10
Grabowski WW, Wang LP. 2013. Growth of cloud droplets in a turbulent environment. *Annu. Rev. Fluid Mech.* 45:293–324
Graeber G, Regulagadda K, Hodel P, Küttel C, Landolf D, et al. 2021. Leidenfrost droplet trampolining. *Nat. Commun.* 12:1727
Hadjiconstantinou NG. 2024. Molecular mechanics of liquid and gas slip flow. *Annu. Rev. Fluid Mech.* 56:435–61
Hamdan KS, Kim DE, Moon SK. 2015. Droplets behavior impacting on a hot surface above the Leidenfrost temperature. *Ann. Nuclear Energy* 80:338–47
Hao J, Lu J, Lee L, Wu Z, Hu G, Floryan JM. 2019. Droplet splashing on an inclined surface. *Phys. Rev. Lett.* 122(5):054501
Harvey D, Burton JC. 2023. Hydrodynamic collapse of the Leidenfrost vapor layer. arXiv:2301.10650 [physics.flu-dyn]. **https://doi.org/10.48550/arXiv.2301.10650**
Harvey D, Harper JM, Burton JC. 2021. Minimum Leidenfrost temperature on smooth surfaces. *Phys. Rev. Lett.* 127(10):104501
He C, Xia X, Zhang P. 2019. Non-monotonic viscous dissipation of bouncing droplets undergoing off-center collision. *Phys. Fluids* 31(5):052004
Heil M, Hazel A, Puneet M. 2022. oomph-lib. *Object-oriented, open-source finite-element library*. **https://github.com/oomph-lib/oomph-lib**
Hicks PD, Purvis R. 2010. Air cushioning and bubble entrapment in three-dimensional droplet impacts. *J. Fluid Mech.* 649:135–63
Hicks PD, Purvis R. 2011. Air cushioning in droplet impacts with liquid layers and other droplets. *Phys. Fluids* 23(6):062104
Hicks PD, Purvis R. 2013. Liquidsolid impacts with compressible gas cushioning. *J. Fluid Mech.* 735:120–49
Hocking LM. 1959. The collision efficiency of small drops. *Q. J. R. Meteorol. Soc.* 85(363):44–50
Hocking LM. 1973. The effect of slip on the motion of a sphere close to a wall and of two adjacent spheres. *J. Eng. Math.* 7(3):207–21
Hocking LM, Jonas PR. 1970. The collision efficiency of small drops. *Q. J. R. Meteorol. Soc.* 96(410):722–29

How MLS, Koch DL, Collins LR. 2021. Non-continuum tangential lubrication gas flow between two spheres. *J. Fluid Mech.* 920:A2
Huang KL, Pan KL. 2021. Transitions of bouncing and coalescence in binary droplet collisions. *J. Fluid Mech.* 928:A7
Jian Z, Josserand C, Popinet S, Ray P, Zaleski S. 2018. Two mechanisms of droplet splashing on a solid substrate. *J. Fluid Mech.* 835:1065–86
Jiang YJ, Umemura A, Law CK. 1992. An experimental investigation on the collision behaviour of hydrocarbon droplets. *J. Fluid Mech.* 234:171–90
Josserand C, Thoroddsen S. 2016. Drop impact on a solid surface. *Annu. Rev. Fluid Mech.* 48:365–91
Josserand C, Zaleski S. 2003. Droplet splashing on a thin liquid film. *Phys. Fluids* 15(6):1650
Kavehpour HP. 2015. Coalescence of drops. *Annu. Rev. Fluid Mech.* 47:245–68
Kaviani R, Kolinski JM. 2023. The characteristic rupture height of the mediating air film beneath an impacting drop on atomically smooth mica. arXiv:2302.12740 [physics.flu-dyn]. **https://doi.org/10.48550/arXiv.2302.12740**
Kolinski JM, Mahadevan L, Rubinstein SM. 2014. Drops can bounce from perfectly hydrophilic surfaces. *Europhys. Lett.* 108(2):24001
Kolinski JM, Rubinstein SM, Mandre S, Brenner MP, Weitz DA, Mahadevan L. 2012. Skating on a film of air: drops impacting on a surface. *Phys. Rev. Lett.* 108(7):074503
Kyobula M, Adedeji A, Alexander MR, Saleh E, Wildman R, et al. 2017. 3D inkjet printing of tablets exploiting bespoke complex geometries for controlled and tuneable drug release. *J. Control. Release* 261:207–15
Langley KR, Li EQ, Thoroddsen ST. 2017. Impact of ultra-viscous drops: air-film gliding and extreme wetting. *J. Fluid Mech.* 813:647–66
Langley KR, Thoroddsen ST. 2019. Gliding on a layer of air: impact of a large-viscosity drop on a liquid film. *J. Fluid Mech.* 878:R2
Law KL, Chu HY. 2019. Bowling water drops on water surface. *Phys. Fluids* 31(6):067101
Lee SH, Harth K, Rump M, Kim M, Lohse D, et al. 2020. Drop impact on hot plates: contact times, lift-off and the lamella rupture. *Soft Matter* 16(34):7935–49
Lesser MB, Field JE. 1983. The impact of compressible liquids. *Annu. Rev. Fluid Mech.* 15:97–122
Li EQ, Vakarelski IU, Thoroddsen ST. 2015. Probing the nanoscale: the first contact of an impacting drop. *J. Fluid Mech.* 785:R2
Li J. 2016. Macroscopic model for head-on binary droplet collisions in a gaseous medium. *Phys. Rev. Lett.* 117(21):214502
Liu D, Tran T. 2020. Size-dependent spontaneous oscillations of Leidenfrost droplets. *J. Fluid Mech.* 902:A21
Liu M, Bothe D. 2019. Toward the predictive simulation of bouncing versus coalescence in binary droplet collisions. *Acta Mech.* 230(2):623–44
Liu Y, Tan P, Xu L. 2015. Kelvin–Helmholtz instability in an ultrathin air film causes drop splashing on smooth surfaces. *PNAS* 112(11):3280–84
Lo HY, Liu Y, Xu L. 2017. Mechanism of contact between a droplet and an atomically smooth substrate. *Phys. Rev. X* 7(2):021036
Ma X, Liétor-Santos JJ, Burton JC. 2017. Star-shaped oscillations of Leidenfrost drops. *Phys. Rev. Fluids* 2(3):031602
Mandre S, Mani M, Brenner MP. 2009. Precursors to splashing of liquid droplets on a solid surface. *Phys. Rev. Lett.* 102(13):134502
Mani M, Mandre S, Brenner MP. 2010. Events before droplet splashing on a solid surface. *J. Fluid Mech.* 647:163–85
Marchand A, Chan TS, Snoeijer JH, Andreotti B. 2012. Air entrainment by contact lines of a solid plate plunged into a viscous fluid. *Phys. Rev. Lett.* 108(20):204501
Maxwell JC. 1879. VII. On stresses in rarified gases arising from inequalities of temperature. *Philos. Trans. R. Soc. Lond.* 170:231–56
Moon JH, Choi CK, Allen JS, Lee SH. 2018. Observation of a mixed regime for an impinging droplet on a sessile droplet. *Int. J. Heat Mass Transf.* 127:130–35
Neitzel GP, Dell'Aversana P. 2002. Noncoalescence and nonwetting behavior of liquids. *Annu. Rev. Fluid Mech.* 34:267–89

Nobari MRH, Tryggvason G. 1996. Numerical simulations of three-dimensional drop collisions. *AIAA J.* 34(4):750–55
Pack M, Hu H, Kim D, Zheng Z, Stone HA, Sun Y. 2017. Failure mechanisms of air entrainment in drop impact on lubricated surfaces. *Soft Matter* 13(12):2402–9
Pan KL, Chou PC, Tseng YJ. 2009. Binary droplet collision at high Weber number. *Phys. Rev. E* 80(3):036301
Pan KL, Law CK. 2007. Dynamics of droplet–film collision. *J. Fluid Mech.* 587:1–22
Pan KL, Law CK, Zhou B. 2008. Experimental and mechanistic description of merging and bouncing in head-on binary droplet collision. *J. Appl. Phys.* 103(6):064901
Pirat C, Lebon L, Fruleux A, Roche JS, Limat L. 2010. Gyroscopic instability of a drop trapped inside an inclined circular hydraulic jump. *Phys. Rev. Lett.* 105(8):084503
Popinet S. 2018. Numerical models of surface tension. *Annu. Rev. Fluid Mech.* 50:49–75
Qian J, Law CK. 1997. Regimes of coalescence and separation in droplet collision. *J. Fluid Mech.* 331:59–80
Quéré D. 2013. Leidenfrost dynamics. *Annu. Rev. Fluid Mech.* 45:197–215
Rayleigh. 1899. XXXVI. Investigations in capillarity. *Lond. Edinb. Dublin Philos. Mag. J. Sci.* 48(293):321–37
Rein M. 1993. Phenomena of liquid drop impact on solid and liquid surfaces. *Fluid Dyn. Res.* 12(2):61–93
Rein M, Delplanque JP. 2008. The role of air entrainment on the outcome of drop impact on a solid surface. *Acta Mech.* 201:105–18
Reitz RD. 2013. Directions in internal combustion engine research. *Combust. Flame* 160(1):1–8
Reynolds O. 1881. On the floating of drops on the surface of water depending only on the purity of the surface. *Proc. Lit. Philos. Soc. Manch.* 21(1):413–14
Reynolds O. 1886. IV. On the theory of lubrication and its application to Mr. Beauchamp tower's experiments, including an experimental determination of the viscosity of olive oil. *Philos. Trans. R. Soc. Lond.* 177:157–234
Riboux G, Gordillo JM. 2014. Experiments of drops impacting a smooth solid surface: a model of the critical impact speed for drop splashing. *Phys. Rev. Lett.* 113(2):024507
Sanjay V, Lakshman S, Chantelot P, Snoeijer J, Lohse D. 2023. Drop impact on viscous liquid films. *J. Fluid Mech.* 958:A25
Schotland RM. 1960. Experimental results relating to the coalescence of water drops with water surfaces. *Discuss. Faraday Soc.* 30:72–77
Sharipov F, Seleznev V. 1998. Data on internal rarefied gas flows. *J. Phys. Chem. Ref. Data* 27(3):657–706
Sharma PK, Dixit HN. 2021. Regimes of wettability-dependent and wettability-independent bouncing of a drop on a solid surface. *J. Fluid Mech.* 908:A37
Shikhmurzaev YD. 2007. *Capillary Flows with Forming Interfaces*. Boca Raton, FL: CRC
Shirota M, van Limbeek MAJ, Lohse D, Sun C. 2017. Measuring thin films using quantitative frustrated total internal reflection (FTIR). *Eur. Phys. J. E* 40(5):54
Shirota M, van Limbeek MAJ, Sun C, Prosperetti A, Lohse D. 2016. Dynamic Leidenfrost effect: relevant time and length scales. *Phys. Rev. Lett.* 116(6):064501
Siewert CE. 2003. The linearized Boltzmann equation: concise and accurate solutions to basic flow problems. *Z. Angew. Math. Phys.* 54(2):273–303
Smith FT, Li L, Wu GX. 2003. Air cushioning with a lubrication/inviscid balance. *J. Fluid Mech.* 482:291–318
Sobac B, Rednikov A, Dorbolo S, Colinet P. 2014. Leidenfrost effect: accurate drop shape modeling and refined scaling laws. *Phys. Rev. E* 90(5):053011. Erratum. 2021. *Phys. Rev. E* 103(3):039901
Sprittles JE. 2015. Air entrainment in dynamic wetting: Knudsen effects and the influence of ambient air pressure. *J. Fluid Mech.* 769:444–81
Sprittles JE. 2017. Kinetic effects in dynamic wetting. *Phys. Rev. Lett.* 118(11):114502
Staat HJJ, Tran T, Geerdink B, Riboux G, Sun C, et al. 2015. Phase diagram for droplet impact on superheated surfaces. *J. Fluid Mech.* 779:R3
Stimson M, Jeffery GB, Filon LNG. 1926. The motion of two spheres in a viscous fluid. *Proc. R. Soc. Ser. A* 111(757):110–16
Struchtrup H. 2005. *Macroscopic Transport Equations for Rarefied Gas Flows. Interaction of Mechanics and Mathematics*. Berlin: Springer
Sundararajakumar RR, Koch DL. 1996. Non-continuum lubrication flows between particles colliding in a gas. *J. Fluid Mech.* 313:283–308

Tang X, Saha A, Law CK, Sun C. 2016. Nonmonotonic response of drop impacting on liquid film: mechanism and scaling. *Soft Matter* 12(20):4521–29

Tang X, Saha A, Law CK, Sun C. 2019. Bouncing drop on liquid film: dynamics of interfacial gas layer. *Phys. Fluids* 31:013304

Thoroddsen ST, Etoh T, Takehara K. 2008. High-speed imaging of drops and bubbles. *Annu. Rev. Fluid Mech.* 40:257–85

Thoroddsen ST, Takehara K, Etoh TG. 2010. Bubble entrapment through topological change. *Phys. Fluids* 22(5):051701

Tran T, Staat HJJ, Prosperetti A, Sun C, Lohse D. 2012. Drop impact on superheated surfaces. *Phys. Rev. Lett.* 108(3):036101

Tryggvason G, Bunner B, Esmaeeli A, Juric D, Al-Rawahi N, et al. 2001. A front-tracking method for the computations of multiphase flow. *J. Comput. Phys.* 169(2):708–59

Usawa M, Fujita Y, Tagawa Y, Riboux G, Gordillo JM. 2021. Large impact velocities suppress the splashing of micron-sized droplets. *Phys. Rev. Fluids* 6(2):023605

van Limbeek MAJ, Hoefnagels PBJ, Shirota M, Sun C, Lohse D. 2018. Boiling regimes of impacting drops on a heated substrate under reduced pressure. *Phys. Rev. Fluids* 3(5):053601

van Limbeek MAJ, Ramírez-Soto O, Prosperetti A, Lohse D. 2021. How ambient conditions affect the Leidenfrost temperature. *Soft Matter* 17(11):3207–15

van Limbeek MAJ, Schaarsberg MHK, Sobac B, Rednikov A, Sun C, et al. 2017. Leidenfrost drops cooling surfaces: theory and interferometric measurement. *J. Fluid Mech.* 827:614–39

Vandre E, Carvalho MS, Kumar S. 2012. Delaying the onset of dynamic wetting failure through meniscus confinement. *J. Fluid Mech.* 707:496–520

Waitukaitis SR, Zuiderwijk A, Souslov A, Coulais C, van Hecke M. 2017. Coupling the Leidenfrost effect and elastic deformations to power sustained bouncing. *Nat. Phys.* 13(11):1095–99

Wang CH, Hung WG, Fu SY, Huang WC, Law CK. 2003. On the burning and microexplosion of collision-generated two-component droplets: miscible fuels. *Combust. Flame* 134(3):289–300

Wanninkhof R, Asher WE, Ho DT, Sweeney C, McGillis WR. 2009. Advances in quantifying air-sea gas exchange and environmental forcing. *Annu. Rev. Mar. Sci.* 1:213–44

Williams H, Sprittles J, Padrino JC, Denissenko P. 2022. Effect of ambient gas on cavity formation for sphere impacts on liquids. *Phys. Rev. Fluids* 7(9):094003

Willis KD, Orme ME. 2000. Experiments on the dynamics of droplet collisions in a vacuum. *Exp. Fluids* 29(4):347–58

Wu X, Saha A. 2022. Droplet impact on liquid films: bouncing-to-merging transitions for two-liquid systems. *Phys. Fluids* 34(10):103313

Xu L, Zhang WW, Nagel SR. 2005. Drop splashing on a dry smooth surface. *Phys. Rev. Lett.* 94(18):184505

Yim E, Bouillant A, Quéré D, Gallaire F. 2022. Leidenfrost flows: instabilities and symmetry breakings. *Flow* 2:E18

Zhang L, Soori T, Rokoni A, Kaminski A, Sun Y. 2021a. Air film contact modes of drop impact on lubricated surfaces under reduced pressures. *Phys. Fluids* 33(9):092110

Zhang L, Soori T, Rokoni A, Kaminski A, Sun Y. 2021b. Thin film instability driven dimple mode of air film failure during drop impact on smooth surfaces. *Phys. Rev. Fluids* 6(4):044002

Zhang L, Soori T, Rokoni A, Sun Y. 2022. Postcontact droplet spreading and bubble entrapment on a smooth surface. *Phys. Rev. Fluids* 7(10):104003

Zhang P, Law CK. 2011. An analysis of head-on droplet collision with large deformation in gaseous medium. *Phys. Fluids* 23(4):042102

Zhang Z, Chi Y, Shang L, Zhang P, Zhao Z. 2016. On the role of droplet bouncing in modeling impinging sprays under elevated pressures. *Int. J. Heat Mass Transf.* 102:657–68

Zhao TY, Patankar NA. 2020. The thermo-wetting instability driving Leidenfrost film collapse. *PNAS* 117(24):13321–28